JGR Atmospheres

RESEARCH ARTICLE
10.1029/2022JD037489

Trend and Interannual Variations of Reactive Nitrogen Deposition in China During 2008–2017 and the Roles of Anthropogenic Emissions and Meteorological Conditions

Mingrui Ma[1], Bo Zheng[2], Wen Xu[3], Jiachen Cao[4], Kaiyue Zhou[1], and Yu Zhao[1,5]

[1]State Key Laboratory of Pollution Control and Resource Reuse, School of the Environment, Nanjing University, Nanjing, China, [2]Institute of Environment and Ecology, Tsinghua Shenzhen International Graduate School, Tsinghua University, Shenzhen, China, [3]College of Resources and Environmental Sciences, National Academy of Agriculture Green Development, China Agricultural University, Beijing, China, [4]School of Environmental Science and Engineering, Nanjing University of Information Science and Technology, Nanjing, China, [5]Jiangsu Collaborative Innovation Center of Atmospheric Environment and Equipment Technology (CICAEET), Nanjing University of Information Science and Technology, Nanjing, China

Abstract Abundant emissions have made China as one of the hotpots of atmospheric reactive nitrogen (Nr) deposition over the world. Here we conducted multi-year simulation and explored the trend and interannual variations (IAVs) of China's Nr deposition for different forms (wet and dry) and species (oxidized and reduced nitrogen, OXN and RDN) during 2008–2017. Sensitivity analysis scenarios were applied to evaluate the roles of anthropogenic emissions and meteorological conditions on the changing deposition. The annual mean Nr deposition was simulated at 15.7 ± 0.9 kg N ha^{-1} yr^{-1} for China. Attributed mainly to the changing OXN, the trend in Nr deposition over the 10-year period showed an inverted "V" pattern, reflecting the benefit of nation actions on NO_X emissions controls. The standard deviation ellipse analysis suggested a clear interannual shift of spatial distribution of Nr deposition to the southwest during 2013–2017. Based on the mean absolute deviation (MAD) and absolute percent departure from the mean obtained in different simulation scenarios, the IAVs of Nr deposition were found to be driven mainly by the changing meteorological conditions, and the correlation coefficient between MADs of Nr deposition and precipitation reached 0.47. Relative to meteorological factor, the changing emissions could explain 61%–83% of 10-year trend of Nr deposition for the concerned regions, thus were identified as the main driver of the trend. The changing meteorological conditions played a more important role on shaping the IAVs of Nr deposition, with the relative contributions estimated at 60% for the concerned regions.

Plain Language Summary Due to abundant anthropogenic emissions, China has been a hotspot of deposition of atmospheric reactive nitrogen (Nr), which exerts multiple ecological and environmental damages. During the past decade, China has been implementing aggressive actions of air pollution controls, leading to large changes in Nr emissions and thereby deposition. The evolution of Nr deposition as well as its major influencing factors is of great concern for both scientific community and policy makers. We conducted numeric simulation and geographic analysis, to explore the spatiotemporal change of Nr deposition and to separate the contributions of anthropogenic (emissions) and natural (meteorological conditions) to the change for 2008–2017. We found a clear growth of Nr deposition till 2012 followed by a decline afterward for the whole country, and unequal changes in different regions resulted in a shift to southwest for the spatial distribution of Nr deposition since 2012. The changing emissions were identified as the major contributor to the trend of Nr deposition, while meteorological conditions played a more important role on its interannual variation. The outcomes improve the understanding of driving forces of the changing Nr deposition in China, and reveal the effectiveness of national pollution controls on it.

Key Points:

- Trend of annual Nr deposition during 2008–2017 showed an inverted "V" pattern, owing to the nation actions of NO_X emission controls
- The spatial heterogeneity of the Nr deposition in China has been weakened, with the deposition gravity shifting to the southwest
- Emission change dominated the 10-year trend of Nr deposition while meteorology played a more important role on its interannual variations

Supporting Information:

Supporting Information may be found in the online version of this article.

Correspondence to:

Y. Zhao,
yuzhao@nju.edu.cn

Citation:

Ma, M., Zheng, B., Xu, W., Cao, J., Zhou, K., & Zhao, Y. (2023). Trend and interannual variations of reactive nitrogen deposition in China during 2008–2017 and the roles of anthropogenic emissions and meteorological conditions. *Journal of Geophysical Research: Atmospheres*, *128*, e2022JD037489. https://doi.org/10.1029/2022JD037489

Received 14 JUL 2022
Accepted 8 MAR 2023

Author Contributions:

Conceptualization: Mingrui Ma, Yu Zhao
Data curation: Mingrui Ma
Formal analysis: Mingrui Ma
Funding acquisition: Yu Zhao
Investigation: Mingrui Ma, Jiachen Cao, Kaiyue Zhou
Methodology: Yu Zhao
Project Administration: Yu Zhao
Resources: Bo Zheng, Wen Xu
Validation: Jiachen Cao, Kaiyue Zhou
Writing – original draft: Mingrui Ma
Writing – review & editing: Mingrui Ma, Bo Zheng, Wen Xu, Jiachen Cao, Kaiyue Zhou, Yu Zhao

1. Introduction

At the global scale, the atmospheric levels of reactive nitrogen (Nr, including oxidized and reduced nitrogen species, OXN and RDN, respectively) have increased explosively after the industrial revolution due to human activities, especially fossil flue consumption and agricultural intensification (Liu & Du, 2020). Increased atmospheric Nr influences air quality through participating in aerosol formation and photochemical reactions, and results in excessive Nr deposition to terrestrial and aquatic ecosystems through both dry and wet pathways. Since 2000s, the average Nr deposition has exceeded 10 kg N ha^{-1} yr^{-1} in many regions of the world, much greater

than the level without the human influence (0.5 kg N ha^{-1} yr^{-1} or smaller) and it is expected to remain stable in the future (Kanakidou et al., 2016). Large amount of Nr deposition can cause adverse ecological effects, such as soil acidification (Liu et al., 2011), eutrophication in water bodies (Matson et al., 2002), forest decline (Yue et al., 2019), and global biodiversity loss (Bobbink et al., 2010; Greaver et al., 2012). In addition, Nr deposition is closely related to the ecosystem carbon cycles and thereby affects the global climate change (Aber et al., 1998; Chen et al., 2015; Liu & Greaver, 2009).

Since late 1970s, China has experienced rapid industrialization and urbanization, and has consumed the fossil fuels and fertilizers at an unprecedented growth rate to meet the increasing needs of the world's largest population (Fowler et al., 2013; Gu et al., 2012; Melillo, 2021). It is reported that the annual NO_X (NO_2 + NO) emissions in China increased rapidly from 11.0 million metric tons (Mt) in the mid-1990s to 26.1 Mt in 2010, and then experienced modest decline by 21% between 2013 and 2017 due to effective implementation of National Action Plan on the Prevention and Control of Air Pollution (NAPPCAP) designed to mitigate air pollution (Zhao et al., 2013; Zheng et al., 2018). Meanwhile, NH_3 emissions were nearly doubled from 2.9 Mt in 1980 to 5.0 Mt in 2012, followed by a slight fluctuation related mainly to variation in agricultural sector (Kang et al., 2016). Enhanced Nr emissions (mainly including NO_X and NH_3) resulted in a high level of atmospheric Nr deposition in China, and made it become one of the Nr deposition hotpots in East Asia and even worldwide (Vet et al., 2014). A series of studies based on available historical observation have estimated long-term trends of national Nr deposition. Liu et al. (2013) showed that the bulk Nr deposition (wet deposition plus part of dry deposition) in China has increased by 60% from 13.2 kg N ha^{-1} yr^{-1} in the 1980s to 21.1 kg N ha^{-1} yr^{-1} in the 2000s. Yu et al. (2019) supplemented the dry deposition estimation by developing a linear relationship between deposition and satellite-derived column of specific species, and reported that the Nr deposition stabilized after 2005. Wen et al. (2020) expanded the Nationwide Nitrogen Deposition Monitoring Network (NNDMN) data to 2018, and found that current levels of bulk and dry Nr deposition (19.4 ± 0.8 and 20.6 ± 0.4 kg N ha^{-1} yr^{-1}, respectively) in China were both approximately twice of those in the United States, Europe, and Japan. Recently, Zhao et al. (2022) developed a generalized additive model by combining the ground observation, satellite-derived column and other meteorological and land-use data, and obtained the national gridded data set of bulk Nr deposition from 2005 to 2020 at a horizontal resolution of 0.25° × 0.25°.

Compared to the abundant ground observation of ambient air pollutant concentrations, the sites of deposition monitoring were relatively sparse, particularly for dry deposition, due to the difficultly and expensiveness of direct measurement methods (e.g., eddy correlation). Even for wet deposition, various sampling procedures and analytical methods applied in different Chinese monitoring networks resulted in great challenge in data quality and comparability assurance (Liu et al., 2020). Such limitations led to bias in statistical modeling based on observation and prevented better estimation of spatiotemporal variations of Nr deposition in China. With the wide application of numerical simulation methods in atmospheric chemistry, three-dimensional atmospheric chemical transport model (CTM) provides a useful tool to better understand the trend of Nr deposition at multiple spatial scales. It calculates the deposition of each Nr species with high temporal and spatial resolution by considering the complex atmospheric process, which can effectively compensate for the insufficient spatial coverage of observation (Flechard et al., 2011; Zhao et al., 2015). A series of studies conducted at national or regional scale for China indicated that high deposition of atmospheric Nr mainly occurred in the eastern regions with developed economy and intensive Nr emissions (Huang et al., 2015; Xu et al., 2018; Zhao et al., 2017). The project of Model Inter-Comparison Study for Asia phase III (MICS-Asia III) reported that annual accumulated Nr deposition over China under multiple CTMs in 2010 ranged from 2,800 to 7,200 Gg, more than the other 12 East Asian countries (Itahashi et al., 2020). Most of the CTM modeling studies focused on single year or short term, while long-term trend of Nr deposition in China has been rarely analyzed. Given China's ambitions and actions in addressing the Nr pollution (Liu et al., 2017), there is a growing research need on the interannual variations (IAVs) of Nr deposition.

Along with continuous efforts of China's air pollution control after 2005, the effectiveness of reduction of anthropogenic air pollutant emissions on air quality has been increasingly concerned by both scientific community and policy makers (Geng et al., 2021). More and more evidences from observational and modeling studies suggested that abatement of SO_2, NO_X, and NH_3 emissions has resulted in declining concentration of fine particulate matter ($PM_{2.5}$) across the country, even with the interannual fluctuation of meteorology (Geng et al., 2019; Xiao et al., 2021). Emission control was also believed to be beneficial for Nr deposition alleviation (Liu et al., 2019). Meanwhile, meteorological conditions, with considerably interannual variations, could play an important role on

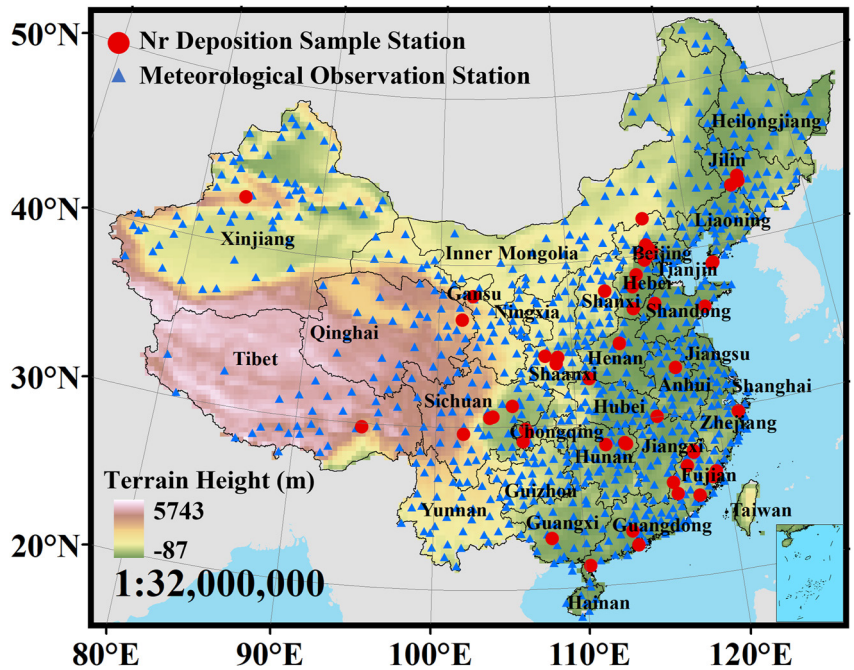

Figure 1. Schematic diagram of the research domain and the locations of monitoring stations. The red dots represent the Nr deposition sample stations and the blue triangle points represent the meteorological observation stations.

the key processes involved in the deposition such as long-range transport and chemical conversion of atmospheric compositions (Civerolo et al., 2008; Liu & Wang, 2020). The emissions and meteorology have jointly resulted in the interannual spatiotemporal change of Nr deposition, but their relative contributions to the change have not been quantified or separated clearly, attributed partly to the lack of long-term modeling studies. Such analysis will be helpful for diagnosing the driving factors of the interannual variations of Nr deposition and evaluating the effectiveness of China's emission control strategy on deposition, for the periods with notable changes in both abundance and composition of Nr due to the strictest ever air pollution prevention actions (e.g., NAPPCAP).

Here we simulated the atmospheric Nr deposition in China from 2008 to 2017 using the EMEP MSC-W model (Meteorological Synthesizing Centre–West of EMEP, the European Monitoring and Evaluation Programme, shortened as EMEP below) by species. We focused on the difference between the two periods, that is, 2008–2012 when the Nr emissions continued to rise, and 2013–2017 when NAPPCAP was implemented. The spatiotemporal changes over the two periods were identified by piecewise linear regression analysis and standard deviation ellipse (SDE) method. The IAVs of Nr deposition and relative contributions of anthropogenic emissions and meteorological changes were assessed based on sensitivity experiment through EMEP model. The outcomes can improve the understanding of key driving factors of atmospheric Nr deposition in China, and serve as scientific basis for better policy making of reducing the ecological risks of Nr deposition.

2. Data and Methods

2.1. Model Description and Evaluation Methods

The EMEP MSC-W CTM was developed by the Norwegian Meteorological Institute to tackle problems of air concentrations and depositions as a whole, including acid deposition, tropospheric ozone, and particles (Simpson et al., 2012). This study used EMEP (version rv4.17) offline coupled with the Weather Research and Forecast (WRF) model (version 3.9.1) as the meteorological driving field. Previous studies have shown the feasibility of coupling between WRF and EMEP model (Ma et al., 2020; van der Swaluw et al., 2021; Werner et al., 2018). The settings of the physical and chemical parameterization schemes are summarized in Table S1 in Supporting Information S1. As shown in Figure 1, the research domain covered the mainland China with a horizontal resolution of 27 km × 27 km. Twenty vertical layers were defined and reached about 100 hPa at the top. The meteorological initial and boundary conditions were obtained from Final Operational Global Reanalysis (FNL) data provided by

the National Centers for Environmental Prediction (NCEP) and the National Center for Atmospheric Research (NCAR) with a horizontal resolution of 1° × 1° (http://rda.ucar.edu/datasets/ds083.2/). For anthropogenic emissions within China, we applied the Multi-resolution Emission Inventory for China (MEIC) (http://www.meicmodel.org/?page_id=560) developed by Tsinghua University (Li, Liu, et al., 2017; Zheng et al., 2018). For the emissions outside of China, we applied the Asian anthropogenic emission inventory, named MIX, developed for the Model Inter-Comparison Study for Asia (MICS-Asia) project (Li, Zhang, et al., 2017). The horizontal resolutions of both emission inventories were 0.25° × 0.25°. The emissions from natural sources included biogenic emissions calculated as a function of underlying surface vegetation species and regional meteorological parameters, sea salt aerosol emissions, and natural mineral dust. More details were archived in Simpson et al. (2012).

Temporal profiles of emissions are fundamental inputs for CTMs and play an important role on the model performance (Wu et al., 2019). The temporal distribution of emissions was determined by country in EMEP model (http://www.emep.int/grid/country_numbers.txt). Unfortunately, current EMEP model did not include the temporal distribution factors specifically for China, and assumed no diurnal variation of emissions, which would increase the simulation uncertainty for the country. To improve the deposition simulation, therefore, we adopted local information on monthly, daily and hourly distribution of emissions for China (He et al., 2018; Li, Liu, et al., 2017; Shen et al., 2015). Briefly, the monthly profiles by sector were developed based on the monthly statistics of fuel consumption and industrial production. The weekly and diurnal profiles were developed based on working schedules, on-site investigation and preliminary field measurements combined with recommended values in the technical manual for Chinese emission inventory development (He et al., 2018). The temporal allocation factors for five major emission factors are shown in Figure S1 in Supporting Information S1. The typical temporal patterns of emissions in China were well captured, including the relatively high emissions from agricultural sector in summer and those from residential sector in winter, reduced emissions from industrial and transportation sectors on weekends, and clear diurnal variations for all sectors.

In order to evaluate the model performance, we collected ground observation data of meteorology and Nr deposition in China from 2008 to 2017. The locations of monitoring stations were presented in Figure 1. The meteorological data were derived from the National Meteorological Information Center of China Meteorological Administration (CMA Meteorological Data Centre, 2022, http://data.cma.cn/data/detail/dataCode/A.0012.0001.html). The daily averaged surface pressure (PRES), wind speed at a height of 10 m (WS_{10}), relative humidity (RH) and temperature at a height of 2 m (T_2) were collected from 839 ground weather stations that contained the continuous 10-year observation data from 2008 to 2017. The observations of annual Nr deposition fluxes were taken from the NNDMN deposition data set (Xu et al., 2018, 2019). Here we select 28 sites for dry deposition fluxes and 53 sites for wet deposition fluxes, for which at least 2-year continuous measurement data were available, to evaluate model performance. The details of monitoring stations of Nr deposition are shown in Table S2 in Supporting Information S1.

Normalized mean bias (NMB) and coefficient of correlation (R) between observation and simulation at monthly scale were used to evaluate the performance of meteorology simulation. NMB, normalized mean errors (NME), root mean square error (RMSE) and R at temporal and spatial scales calculated with Equations 1–5, respectively, were used to evaluate the annual Nr deposition simulation:

$$\mathrm{NMB} = \sum_{i=1}^{n}(S_i - O_i) / \sum_{i=1}^{n} O_i \times 100\% \tag{1}$$

$$\mathrm{NME} = \sum_{i=1}^{n}|S_i - O_i| / \sum_{i=1}^{n} O_i \times 100\% \tag{2}$$

$$\mathrm{RMSE} = \sqrt{\frac{1}{n}\sum_{i=1}^{n}(S_i - O_i)^2} \tag{3}$$

$$\text{Temporal } R = \sum_{i=1}^{n}\left(S_i - \overline{S}\right)\left(O_i - \overline{O}\right) / \sqrt{\sum_{i=1}^{n}\left(S_i - \overline{S}\right)^2\left(O_i - \overline{O}\right)^2} \tag{4}$$

$$\text{Spatial } R = \sum_{j=1}^{m}\left(\overline{S}_j - \overline{S_j}\right)\left(\overline{O}_j - \overline{O_j}\right) / \sqrt{\sum_{j=1}^{m}\left(S_j - \overline{S_j}\right)^2\left(O_j - \overline{O_j}\right)^2} \tag{5}$$

where S and O are the annual deposition from model simulation and observation, respectively, $\overline{S}$ and $\overline{O}$ are the annual mean deposition from model simulation and observation, respectively, i and j indicates the individual year or site.

2.2. Evaluation of Relative Contributions of Different Factors to the Changing Deposition

To evaluate the IAVs of atmospheric Nr deposition as well as their contributors over 2008–2017, we performed the following simulation scenarios of atmospheric Nr deposition in China using the WRF-EMEP model and the simulation for each year was conducted from 1st December of the last year to 31st December of the target year, and the first 31 days were treated as a spin-up time.

ANNall: the scenario to examine the IAVs of atmospheric Nr deposition. The meteorological conditions and emissions of anthropogenic and biomass burning origin were allowed to vary from 2008 to 2017.

ANNmeto17: the scenario to examine the influence of the changed emissions on the IAVs of atmospheric Nr deposition. The emissions were allowed to vary from 2008 to 2017, while the meteorological conditions were kept at the level of 2017.

ANNemis17: the scenario to examine the influence of meteorological variations on the IAVs of atmospheric Nr deposition. The meteorological conditions were allowed to vary from 2008 to 2017 while the anthropogenic emissions were kept at the level of 2017.

The mean absolute deviation (MAD) and absolute percent departure from the mean (APDM), which have been widely applied to diagnose the drivers of ambient concentration of air pollutants in previous studies (Mao et al., 2016; Mu & Liao, 2014; Yang et al., 2015; Zhu et al., 2017), were calculated and compared for the three simulation experiments to explore the influences of meteorological and emission changes on IAVs of Nr deposition:

$$\mathrm{MAD} = \frac{1}{n}\sum_{i=1}^{n}\left|F_i - \frac{1}{n}\sum_{i=1}^{n}F_i\right| \tag{6}$$

$$\mathrm{APDM} = \mathrm{MAD}/\left(\frac{1}{n}\sum_{i=1}^{n}F_i\right) \times 100\% \tag{7}$$

where F_i means the Nr deposition flux in year i, and n represents the number of years examined ($n = 10$ in this study). The MAD represents the absolute IAVs in Nr deposition flux while the APDM represent the IAVs relative to the average deposition flux over n years.

To estimate the temporal trend of Nr deposition, linear regression with the least square approach was conducted for the simulated annual Nr deposition against year, and the slope of linear regression was determined as the interannual change rate (ICR, Tg N yr^{-1} or kg N ha^{-1} yr^{-1}) of Nr deposition. Positive (negative) slope indicates increasing (decreasing) trend within the research period. For each species and deposition forms (dry or wet), the deviation from the mean (DM) was calculated to evaluate the annual fluctuation of Nr deposition:

$$\mathrm{DM}_i = \left(F_i - \frac{1}{n}\sum_{i=1}^{n}F_i\right)/\frac{1}{n}\sum_{i=1}^{n}F_i \tag{8}$$

where F_i means the Nr deposition flux in year i, and n represent the number of years examined ($n = 10$ in this study).

We referred to the methodology of Dang et al. (2021) to calculated the normalized contribution of emission or meteorological condition changes to the 10-year trend of Nr deposition during 2008–2017. The specific equations were as follows:

$$\mathrm{CT}_{\mathrm{emis}} = \frac{|\mathrm{ICR}_{\mathrm{ANNmeto17}}|}{(|\mathrm{ICR}_{\mathrm{ANNmeto17}}| + |\mathrm{ICR}_{\mathrm{ANNemis17}}|)} \times 100\% \tag{9}$$

$$\mathrm{CT}_{\mathrm{meto}} = \frac{|\mathrm{ICR}_{\mathrm{ANNemis17}}|}{(|\mathrm{ICR}_{\mathrm{ANNmeto17}}| + |\mathrm{ICR}_{\mathrm{ANNemis17}}|)} \times 100\% \tag{10}$$

where $\mathrm{CT}_{\mathrm{emis}}$ and $\mathrm{CT}_{\mathrm{meto}}$ are the relative contributions of emission and meteorological condition change to trend of Nr deposition, respectively; and $\mathrm{ICR}_{\mathrm{ANNmeto17}}$ and $\mathrm{ICR}_{\mathrm{ANNemis17}}$ represent the ICR of Nr deposition (i.e., the slope obtained from linear regression of Nr deposition against time) for the two simulation scenarios, respectively.

The normalized contributions of the two factors to IAVs of Nr deposition were calculated referred to Fu et al. (2019), and the specific equations were as follows:

$$\mathrm{CI}_{\mathrm{emis}} = \frac{\mathrm{MAD}_{\mathrm{ANNmeto17}}}{(\mathrm{MAD}_{\mathrm{ANNmeto17}} + \mathrm{MAD}_{\mathrm{ANNemis17}})} \times 100\% \tag{11}$$

$$CI_{meto} = \frac{MAD_{ANNemis17}}{(MAD_{ANNmeto17} + MAD_{ANNemis17})} \times 100\% \quad (12)$$

where CI_{emis} and CI_{meto} are the relative contribution of emissions and meteorological conditions to IAVs of Nr deposition, respectively; $MAD_{ANNmeto17}$ and $MAD_{ANNemis17}$ represent the MADs of Nr deposition obtained from different simulation scenarios.

2.3. SDE Method

The spatial evolution of atmospheric Nr deposition in mainland China for the two periods was conducted with a SDE method, which was increasingly applied to explore the spatial variation of emissions (Chen et al., 2019, 2021; Yang et al., 2020), ambient concentration (Peng et al., 2016; Shi, Matsunaga, Yamaguchi, Zhao, et al., 2018; Shi, Matsunaga, Yamaguchi, et al., 2018) and deposition (Ma et al., 2020) of typical atmospheric species.

The SDE method estimates the geospatial pattern by determining the distribution and orientation of a set of two-dimensional datasets, with the specific indicators represented by the average center, SDE, the length of major and minor axis and azimuth (Gong, 2002; Wachowicz & Liu, 2016). Detailed equations and parameters are described in Text Section 1 in the Supplement. Briefly, the ellipse center point is determined first by calculating the weighted average of discrete values in *X* and *Y* directions, and then the ellipse is obtained by calculating the standard distances in *X* and *Y* directions of other points from the average center (Wang et al., 2015). By comparing changes between SDEs of multiple years based on the ANNall simulation, the spatial evolution of Nr deposition can be illustrated. The moving of the average center reveals the overall evolutionary track of Nr deposition; the azimuth change indicates the spatial rotation of ellipse and reflects the deposition change in spatial direction; and the changes in the lengths of the major and minor axes of the ellipse indicate the expansion or shrinking of Nr deposition in specific directions.

3. Results and Discussion

3.1. Evaluation of Nr Deposition Simulation

The performance of meteorological parameter simulation is shown in Figure S2 in Supporting Information S1. Satisfying modeling performance was achieved for PRES, RH and T_2 with the NMBs calculated at −2.0%, 2.3%, and −2.7%, respectively. The monthly WS_{10} were generally overestimated with the NMB calculated at 23.6%. The surface wind speed is usually difficult to simulate with a common systematic overestimation, due to the smoothing of complex underlying surface conditions in mesoscale numerical weather prediction (NWP) models, coupled with the strong turbulence mixing consideration in planetary boundary layer scheme and inaccuracy of global reanalysis driven data (Carvalho et al., 2012; Yu et al., 2017). More recently, multi-year WRF simulations by Liu et al. (2020) and Shen et al. (2021) also showed similar levels of overestimation, with NMB values of 17.9% and 27.0%, respectively. The R^2 were all greater than 0.60, indicating the simulation was in good agreement with observation. In general, WRF well simulated the changes of 2 m temperature, 2 m RH, 10 m wind speed and atmospheric pressure at monthly scale.

The simulated spatial distribution of annual Nr deposition averaged over 2008–2017 and the bias between simulation and observation at site level are shown in Figure 2 by form (dry and wet) and species (oxidized and reduced). Table S3 in Supporting Information S1 summarizes the model performance of annual Nr deposition simulation indicated by NMBs and NMEs for each year. Nr deposition was generally underestimated compared with observation, and the biases for most sites were within −5–0 kg N ha^{-1} yr^{-1} (Figure 2). The NMBs averaged over all the available sites at annual scale ranged from −26% to −3% for different deposition forms and species, while NME ranged from 41% to 53%. The coefficients of variation (CV) of NME, calculated as the standard deviation divided by the average of NME for the 10 years, ranged from 0.08 to 0.19 for various species and forms (Table S3 in Supporting Information S1). The relatively small CVs implied a similar model performance of Nr deposition for different years.

Among them, the NMB for dry deposition of OXN (DDEP_OXN) was −18.00%, while larger underestimation was found for RDN (DDEP_RDN) with the NMB at −30.63%. Since gaseous NH_3, the largest contributor to DDEP_RDN (Wen et al., 2020; Xu et al., 2015), tends to deposit in regions close to emission sources due to its very short lifetimes (generally a few hours, Hertel et al., 2006), the uncertainty of the NH_3 emission inventory

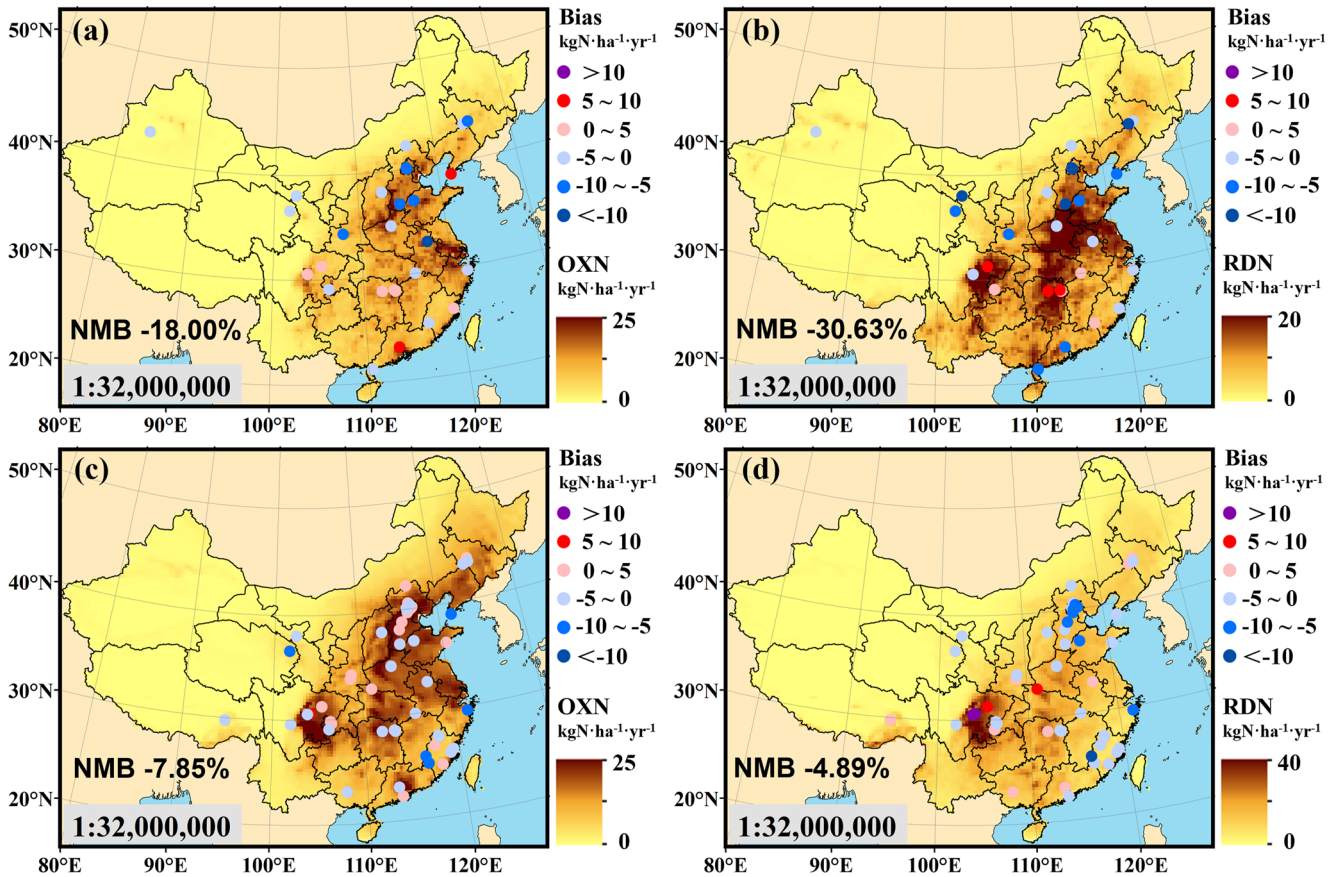

Figure 2. The spatial distribution of annual dry (a, b) and wet (c, d) Nr deposition fluxes (kg N ha^{-1} yr^{-1}) of oxidized nitrogen and reduced nitrogen in ANNvall simulation averaged over 2008–2017. The dots represent the bias between simulation and observation at site level.

could be an important reason for the underestimation. Through satellite constraint, Zhang et al. (2018) estimated that the "bottom-up" methodology could underestimate China's NH_3 emissions by approximately 40% due to lack of detailed activity data and emission factors. Better model performance was achieved for wet deposition. The NMB of oxidized and RDN of wet deposition (WDEP_OXN and WDEP_RDN) were calculated at −7.85% and −4.89%, respectively. It should be noted, however, that most of wet deposition observation actually measured bulk deposition, which included both wet deposition and part of dry deposition (Xu et al., 2015). Therefore, those negative NMBs resulted partly from the inclusion of part of dry deposition and thereby overestimation of wet deposition through bulk deposition observation.

Due to the differences in model framework and deposition algorithms, the performance of Nr deposition simulation with different models varied, mainly for the dry deposition (Chang et al., 2020). Recently, Ge et al. (2020) reported and compared the performances of Nr deposition simulation with multiple models over China based on project of The Model Inter-Comparison Study for Asia (MICS-Asia) phase III. The overall NMBs and NMEs ranged −6.8%–67.2% and 48.3%–82.2% for OXN, and −69.5%––28.6% and −71.7%–44.3% for RDN, respectively (Table 1). The model performance in this work was comparable to previous studies. In addition, Figures S3 and S4 in Supporting Information S1 shows the RMSE and *R* between simulation and observation at the site level, respectively. The RMSEs were less than 6 kg N ha^{-1} yr^{-1} at most sites for different forms and Nr species, and the site-averaged temporal *R* and the spatial *R* were both greater than 0.6. Overall, the WRF-EMEP model reproduced well the observed Nr deposition fluxes in magnitude and spatiotemporal distribution.

3.2. Annual Atmospheric Nr Deposition and Its 10-Year Trend

Table S4 in Supporting Information S1 summarizes the simulated atmospheric Nr deposition for different forms and species averaged over 2008–2017 with WRF-EMEP. The annual mean Nr deposition flux for the 10 years

Table 1
Multi-Model Simulation Performance of Nr Deposition Over China

	CMAQ[a]		NAQPMS		NHM-Chem		GEOS-Chem		EMEP (this study)	
Model	OXN	RDN	OXN	RDN	OXN	RDN	OXN	RDN	OXN	RDN
NMB (%)	−6.8–55.4	−55.1–28.6	67.2	−69.5	0.6	−33.1	0.1	−31.6	−12.9	−17.8
NME (%)	54.3–77.8	49.6–58.7	82.2	71.7	49.5	48.5	48.3	44.3	40.0	48.3

[a]The results of CMAQ model contains different version (v4.7.1 and v5.0.2) and different combinations of scheme.

was simulated at 15.7 ± 0.9 kg N ha^{-1} yr^{-1} for mainland China, comparable with other studies for similar research period. Based on GEOS-Chem simulation and the Kriging interpolation, Zhao et al. (2017) and Yu et al. (2019) reported the mean value of Nr deposition at 16.4 kg N ha^{-1} yr^{-1} for 2008–2012 and 20.4 ± 2.6 kg N ha^{-1} yr^{-1} for 2011–2015, respectively. At the national scale, more Nr was estimated to be removed through wet deposition than dry deposition, with a proportion of 57% of the total deposition (8.6 ± 0.6 out of 15.0 ± 0.8 Tg N yr^{-1}) for the former. The observation data from nationwide network provided a similar proportion with 55% contribution of wet deposition (Xu et al., 2015). For different species, more RDN deposition was found over China than OXN (9.0 ± 0.2 vs. 5.9 ± 0.6 Tg N yr^{-1}), reflecting the large abundance of NH_3 emissions coming mostly from agricultural activities in China.

Figure S5 and Table S5 in Supporting Information S1 show the monthly and seasonal Nr deposition in China averaged over 2008–2017, respectively. Maximum Nr deposition was found in summer and minimum in winter, with their contributions at 5.2 Tg N yr^{-1} (35%) and 2.7 Tg N yr^{-1} (18%) to the annual total deposition of 15.0 Tg N yr^{-1}, respectively. The largest wet deposition of OXN and RDN in summer resulted partly from the highest precipitation in the season. Higher dry deposition of RDN was found in spring, summer and autumn than winter, with the peak flux in summer. Busy agricultural activities are generally prevalent over the three seasons in China, with the NH_3-fertilizers are intensively used on the cropland (Li, Liu, et al., 2017, 2021). In addition, the high temperature in summer accelerated the volatilization of chemical fertilizers, animal manure, urban garbage, and NH_3 from vehicle driving (Pan et al., 2018). Insignificant monthly variation was found for OXN deposition, with relatively higher flux in autumn and winter. It could be partly related to the elevated NO_X emissions from heating in northern China and the enhanced formation of secondary nitrate aerosols during haze pollution that occurred more frequently in colder seasons.

Figure 3a shows the annual atmospheric Nr deposition during 2008–2017 for mainland China. The seasonal variations and inter-annual changes of Nr deposition of different forms and species for the two periods (2008–2012 and 2013–2017) were quantified using the least square piecewise fit approach and summarized in Table 2. An increasing trend over 2008–2012 followed by a decline during 2013–2017 was found for all the species. The annual deposition of DDEP_OXN, DDEP_RDN, WDEP_OXN and WDEP_RDN was estimated to increase by 19%, 4%, 31%, and 10% from 2008 to 2012, and then to decline by 22%, 2%, 23%, and 4% from 2013 to 2017, respectively. As a result, the annual total Nr deposition increased significantly from 14.6 Tg N in 2008 to 16.7 Tg N in 2012, and then declined by 3.11 Tg N (8.6%) in the following 5 years.

With changes in both meteorological conditions and anthropogenic emissions in ANNall simulation, the ICR in deposition of DDEP_OXN, DDEP_RDN, WDEP_OXN, WDEP_RDN, and total Nr deposition over 2008–2012 were +0.15, +0.03, +0.23, +0.10, and +0.51 Tg N yr^{-1}, while those over 2013–2017 were −0.16, −0.02, −0.18, −0.03, and −0.39 Tg N yr^{-1}, respectively. OXN dominated the temporal trend in Nr deposition over the 10-year period. Although RDN was larger than OXN, the ICR of RDN deposition was limited attributed mainly to the small change in anthropogenic NH_3 emission during the study period (3% over 2008%–2012% and −4% over 2013–2017) compared to that of NO_X emissions (21% over 2008%–2012% and −21% over 2013–2017, Figure S6 and Table S6 in Supporting Information S1). Although the highest deposition existed in summer (Table 2 and Table S5 in Supporting Information S1), the contribution to interannual trend of Nr deposition was not significantly larger for summer compared to other seasons. For instance, while the simulated Nr deposition in summer accounted for 35% of the annual level averaged over 2008–2012, the ICR in summer Nr deposition was estimated at +0.15 Tg N yr^{-1}, which contributed only 29% to the growth of annual Nr deposition (+0.51 Tg N yr^{-1}). Relatively great contributions of other seasons to ICR, especially for winter, were partly associated with the big changes in NO_X emissions. As shown in Table S6 in Supporting Information S1, for example, the largest

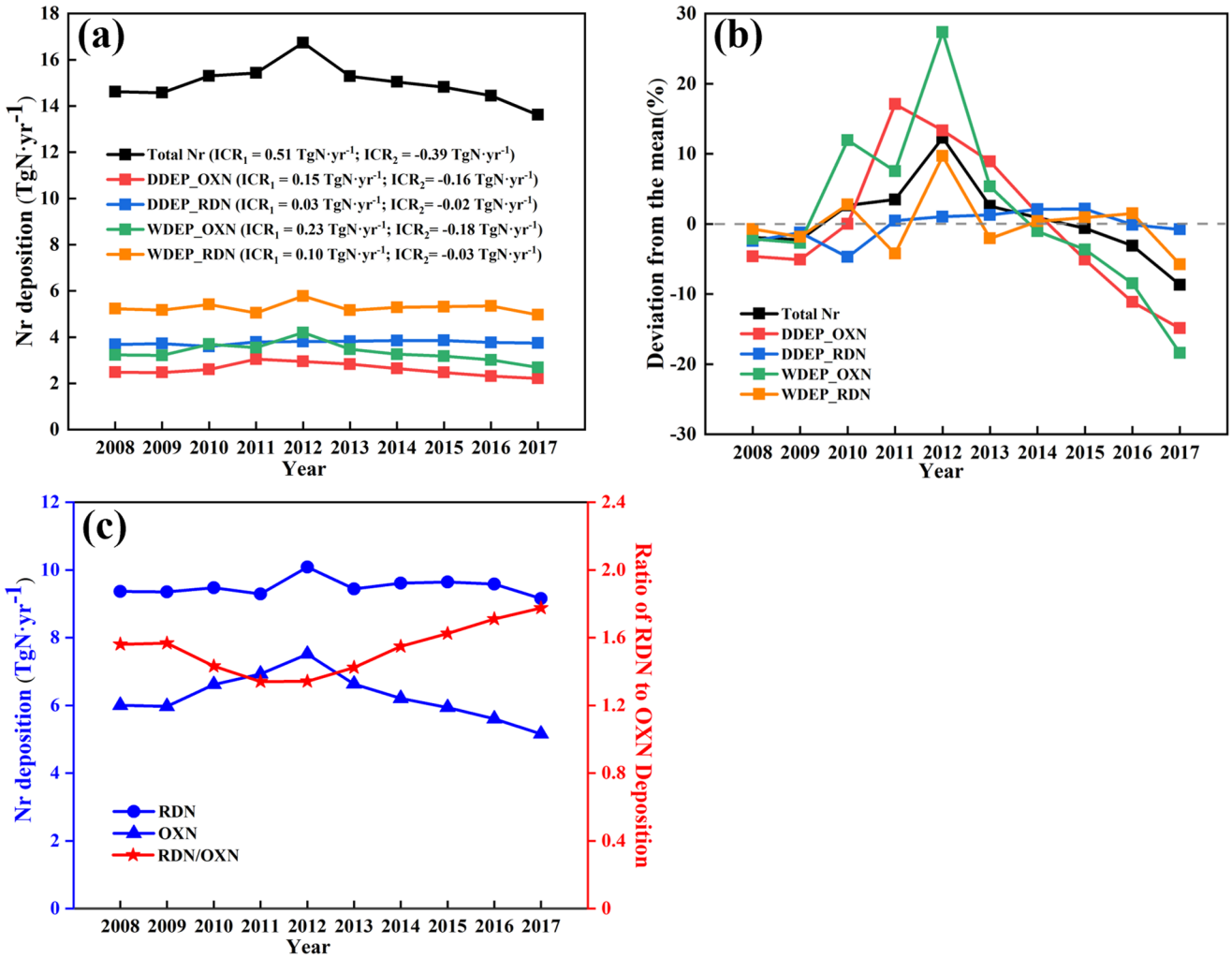

Figure 3. (a) Annual Nr deposition (Tg N) during 2008–2017 for Mainland China. The temporal trends of Nr deposition in two periods (2008–2012 and 2013–2017), indicated by the relative change rate (ICR_1 and ICR_2, Tg N yr^{-1}), are calculated by the least square fit; (b) deviation from the mean of Nr deposition obtained through ANNall simulation; (c) Annual oxidized and reduced nitrogen (OXN and RDN) deposition and the ratio of RDN to OXN deposition during 2008–2017.

ICR of NO_X emissions were found in winter for 2008–2012 (+0.19 Tg N yr^{-1}), attributed probably to the growing demand of heating and thereby elevated coal burning in cold season. Along with the penetration of clean fuel for residential heating, moreover, NO_X emissions were estimated to decline fastest in winter during 2013–2017, indicated by the smallest ICR (−0.18 Tg N yr^{-1}) among all seasons.

Figure 3b shows the DM of Nr deposition obtained through ANNall simulation. From 2008 to 2017, the DMs for all deposition forms generally changed from negative to positive and then dropped back to negative, suggesting an inverted "V" pattern in Nr deposition for the period. The largest variation in DM was found for WDEP_OXN, with the value increasing from −3.7% in 2008 to +25.7% in 2012 and declining to −19.9% in 2017.

Regarding the difference between species, the ratio of RDN to OXN deposition was estimated to increase at 8%·yr^{-1} from 2012 to 2017 compared to a 6%·yr^{-1} decline from 2008 to 2011 (Figure 3c), which could also be supported by the observed significantly increasing ratio of RDN to OXN in total deposition after 2010 at nationwide monitoring sites (Wen et al., 2020). The rising RDN to OXN ratio was expected to be largely driven by the continuous NO_X emission controls after 2010 (e.g., the stringent measures in NAPPCAP), and highlighted the benefits of those measures on limiting atmospheric OXN pollution. The analysis indicated that the Nr pollution in China has been stepping into the RDN dominating condition along with successful control of NOX emissions, and that the strategy on NH_3 emission abatement is urgently needed to alleviate current nitrogen pollution problem. Compared to NOX that came mostly from large-scale fossil fuel burning, NH_3 came widely

Table 2
Simulated Seasonal and Annual Nr Deposition (Tg N) of Different Forms and Species in Years 2008, 2012, 2013, and 2017 in ANNall

		2008–2012			2013–2017		
Form_species	Season[a]	2008	2012	ICR	2013	2017	ICR
DDEP_OXN	Spring	0.57	0.70 (23%)	0.03	0.67	0.52 (−22%)	−0.04
	Summer	0.60	0.70 (17%)	0.04	0.62	0.49 (−21%)	−0.04
	Autumn	0.65	0.75 (15%)	0.04	0.74	0.59 (−20%)	−0.04
	Winter	0.64	0.79 (23%)	0.05	0.79	0.59 (−25%)	−0.05
	Annual	2.46	2.93 (19%)	0.16	2.81	2.20 (−22%)	−0.17
DDEP_RDN	Spring	0.86	0.90 (5%)	0.01	0.90	0.88 (−2%)	−0.01
	Summer	1.09	1.10 (1%)	0.00	1.07	1.06 (−1%)	0.00
	Autumn	0.92	0.96 (4%)	0.01	0.96	0.96 (0%)	0.00
	Winter	0.85	0.88 (4%)	0.01	0.93	0.87 (−6%)	−0.01
	Annual	3.71	3.84 (4%)	0.03	3.85	3.77 (−2%)	−0.02
WDEP_OXN	Spring	0.79	1.01 (28%)	0.05	0.88	0.65 (−26%)	−0.05
	Summer	1.20	1.48 (23%)	0.08	1.28	1.00 (−22%)	−0.07
	Autumn	0.70	0.92 (31%)	0.06	0.81	0.66 (−19%)	−0.03
	Winter	0.51	0.75 (47%)	0.04	0.47	0.34 (−28%)	−0.03
	Annual	3.19	4.17 (31%)	0.23	3.44	2.66 (−23%)	−0.18
WDEP_RDN	Spring	1.35	1.52 (13%)	0.02	1.45	1.30 (−10%)	−0.02
	Summer	2.29	2.42 (6%)	0.03	2.21	2.24 (1%)	0.00
	Autumn	0.97	1.08 (11%)	0.02	0.98	0.98 (0%)	0.00
	Winter	0.64	0.79 (23%)	0.02	0.54	0.48 (−11%)	−0.01
	Annual	5.25	5.80 (10%)	0.10	5.18	4.99 (−4%)	−0.03
Total Nr	Spring	3.57	4.13 (16%)	0.11	3.90	3.34 (−14%)	−0.12
	Summer	5.17	5.70 (10%)	0.15	5.18	4.80 (−7%)	−0.11
	Autumn	3.24	3.71 (15%)	0.13	3.47	3.19 (−8%)	−0.07
	Winter	2.64	3.21 (22%)	0.12	2.73	2.28 (−16%)	−0.09
	Annual	14.62	16.75 (15%)	0.51	15.29	13.62 (−11%)	−0.39

Note. Percentage changes in Nr deposition for 2012–2017 compared to 2008–2013 are shown in brackets. The temporal trends of Nr deposition in two periods (2008–2012 and 2013–2017), indicated by the interannual change rate (ICR, Tg N yr^{-1}), are obtained by the linear regression with least square approach.

[a]Season: Spring includes March, April, and May; Summer includes June, July, and August; Autumn includes September, October, and November; Winter includes December, January, and February.

from nitrogen-fertilizer use and livestock farming that were relatively difficult to be monitored and managed. Similar result was also reported for the United States, where RDN was observed to replace OXN to be the dominant species in inorganic nitrogen deposition within 20 years, based on a nationwide monitoring network (Li et al., 2016; Tan et al., 2020). The common experiences in Nr pollution control for the two countries revealed the great challenge of NH_3 emission abatement for further reducing Nr deposition as well as other negative environmental impacts like secondary particle formation (Liu et al., 2019).

3.3. Spatiotemporal Evolution of Nr Deposition

A clear gradient from west to east was found for all deposition forms and species (Figure 2), driven mainly by the spatial distributions of NH_3 and NO_X emissions (Han et al., 2017; Yu et al., 2019; Zhao et al., 2017). Within Eastern China (EC, 22–41°N, 102–122°E), we defined three key regions covering major hotspots of Nr deposition, including North China (NC, 32–42°N, 110–120°E), South China (SC, 22–32°N, 110–120°E), and the Sichuan

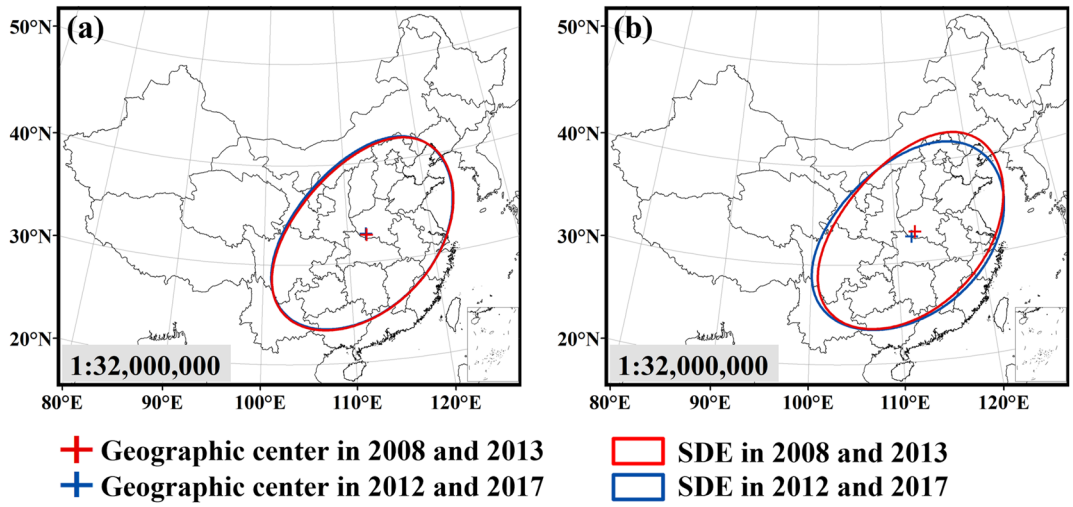

Figure 4. The geographic center and standard deviation ellipse of Nr deposition across mainland China from ANNall simulation during 2008–2012 (a) and 2013–2017 (b).

Basin (SCB, 27–33°N, 102–110°E, Figure S7 in Supporting Information S1). The Nr deposition level in the three regions was more than twice of the national average (Table S4 in Supporting Information S1). For western China (WC, 28–47°N, 78–102°E), the deposition was usually less than 2 kg N ha^{-1} yr^{-1} and kept stable within the research period. High values of DDEP_OXN appeared mainly in EC, especially the Beijing-Tianjin-Hebei, Yangtze River Delta, and Pearl River Delta regions (Figure S7 in Supporting Information S1), resulting mainly from the large NO_X emissions caused by active industrialization and urbanization in those regions. In addition, the urban expansion increased surface roughness and in turn reduced near-surface turbulent diffusion, leading to elevated deposition of air pollutants. High values of DDEP_RDN appeared mainly in NC and SCB with intensive agricultural activities. The appearance of WDEP_OXN covered broad areas of EC influenced by precipitation and atmospheric circulation, while the highest value of WDEP_RDN was found in SCB, under the joint effect of abundant rainfall and local agricultural NH_3 emissions.

Figure 4 shows the changing spatial pattern of Nr deposition across mainland China during 2008–2012 (a) and 2013–2017 (b), indicated by the average center, axis length and rotation angle of SDE. The corresponding parameters of SDEs for individual years are summarized in Table 3. During 2008–2012, there was no significant spatial movement in the Nr deposition over China, with the basically overlapped ellipses for 2008 and 2012. The geographic center of Nr deposition distribution was located at the border of Hubei and Henan provinces. However, a clear shift to the southwest was detected with the center changed from (112.33°N, 33.06°E) to (111.88°N, 32.59°E) during 2013–2017, driven by the unequal variation of deposition in different regions. Table S7 in Supporting Information S1 provides the annual mean Nr deposition in EC, WC, NC, SC. and SCB regions and the relative changes over the two periods. Similar relative changes in Nr deposition were estimated for each region between 2008 and 2012, resulting in the limited variation in the geographic distribution of Nr deposition. For 2013–2017, a downward trend was found for Nr deposition at the national scale with the relative change at 11%. In contrast, there was basically no change in WC, triggering the movement of the average center to the west. Meanwhile, NC was the only region with a relative change larger than the national level at 15%, triggering the movement of the average center to the south.

Table 3
Statistics of Standard Deviation Ellipse Parameters for Years 2008, 2012, 2013, and 2017

Period	Center *X* (°)	Center *Y* (°)	*X* distance (km)	*Y* distance (km)	Azimuth angle (°)
2008	112.26	32.74	106.43	63.84	56.43
2012	112.17	32.85	105.92	64.86	56.61
2013	112.33	33.06	109.22	65.11	56.65
2017	112.10	32.59	107.87	66.64	61.80

Note. Center *X* and Center *Y* represent the longitude and latitude of SDE center point, respectively; *X* distance and *Y* distance mean the length of major and minor axes of the SDEs for individual years, respectively.

The azimuth angles of the SDEs ranged between 0° and 90° for the both periods, indicating that the overall directional distribution of Nr deposition was northeast-southwest. The azimuth angle increased clockwise from 56.65° in 2013 to 61.80° in 2017, implying a diminishing influence of northern China on the distribution and orientation of Nr deposition. The major axes of the ellipse decreased from 109.22 to 107.87 km, and the minor axes increased from 65.11 to 66.64 km. Therefore, the ratio of the major to

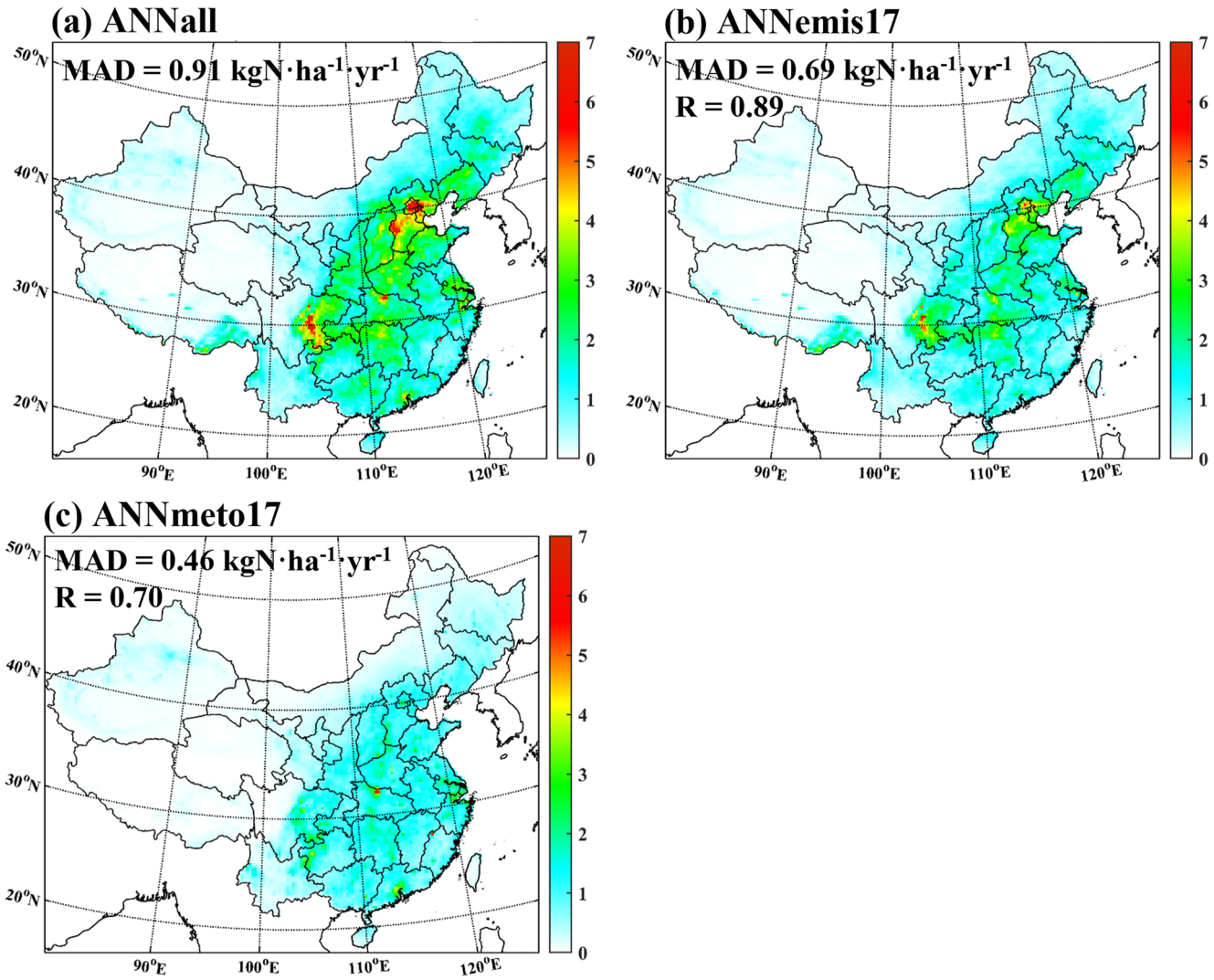

Figure 5. The spatial distribution of mean absolute deviations (kg N ha^{-1} yr^{-1}) of Nr deposition flux simulated in ANNall (a), ANNemis17 (b) and ANNmeto17 (c) during 2008–2017. Domain-averaged mean absolute deviation are presented in each panel and the spatial correlation (*R*) between ANNemis17/ANNmeto17 and ANNall are shown in panel (b) and (c)

minor axes decreased from 1.68 to 1.62, suggesting a shifting in spatial distribution of Nr deposition, from the northeast-southwest direction to a more uniform distribution during 2013–2017. Overall, the shape change of the Nr deposition ellipse between 2013 and 2017 implied that implementation of NAPPCAP weakened the spatial heterogeneity of Nr deposition across the country, by cutting more NO_X emissions in the pollution hotspot with intensive industry and fossil fuel consumption, for example, NC. Indicated by MEIC, the annual NO_X emissions in NC were estimated to decline 22% from 2013 to 2017, much faster than those in WC at 8% (Zheng et al., 2018). The unequal abatement of emissions across the country thus reduced the difference between regions and contributed to the shift of spatial distribution of Nr deposition.

3.4. Relative Contributions of Emission and Meteorological Changes to IAVs and Trend of Nr Deposition

Figure 5a shows the spatial distribution of MAD of Nr deposition during 2008–2017. The MADs of Nr deposition obtained from ANNall simulation ranged 0.01–9.20 kg N ha^{-1} yr^{-1} in China during study period, with an annual average of 0.91 kg N ha^{-1}. MAD of Nr deposition was less than 0.05 kg N ha^{-1} yr^{-1} in most of WC, while larger MAD was estimated for EC. In particular, the strongest IAVs occurred in BTH and SCB, with the MADs exceeding 6 kg N ha^{-1} yr^{-1} for some areas. To further examine the seasonal IAVs of Nr deposition for different

Table 4
The Seasonal Domain-Averaged Mean Absolute Deviations (kg N ha^{-1} yr^{-1}) of Nr Deposition Flux Over NC, SC, and SCB During 2008–2017 in ANNall Simulation

	Spring			Summer			Autumn			Winter		
	NC	SC	SCB	NC	SC	SCB	NC	SC	SCB	NC	SC	SCB
DDEP_OXN	0.15	0.16	0.09	0.25	0.11	0.08	0.18	0.14	0.09	0.11	0.24	0.20
DDEP_RDN	0.10	0.10	0.09	0.13	0.13	0.14	0.11	0.10	0.12	0.11	0.12	0.13
WDEP_OXN	0.39	0.32	0.30	0.70	0.31	0.32	0.48	0.25	0.34	0.24	0.34	0.39
WDEP_RDN	0.43	0.43	0.54	0.83	0.56	0.71	0.48	0.29	0.61	0.24	0.30	0.52
Total Nr	0.85	0.73	0.84	1.62	0.89	1.04	1.03	0.53	0.94	0.49	0.69	0.92

forms and species in key regions, the domain-averaged MADs for NC, SC, and SCB are presented by season in Table 4. In general, the MADs of wet deposition were much higher than that of dry deposition, indicating that IAVs of precipitation could be an important factor affecting that of Nr deposition. The seasonal mean MADs of the Nr deposition ranged 0.53–1.62 kg N ha^{-1} yr^{-1} over the three regions, and the largest MADs were found for summer. Across EC, high convective instability of the warm and moist air resulted in abundant precipitation with strong fluctuation in summer (Zhu et al., 2021). As shown in Figure S8 in Supporting Information S1, the largest MAD of precipitation was found in summer, leading to the strong IAVs of Nr deposition in the season. Regarding the regional difference, higher MADs were found for NC than another two regions for all seasons except winter.

In order to quantify the effects of changing emissions and meteorology on IAVs of Nr deposition, we calculated the MADs of ANNemis17 (Figure 5b) and ANNmeto17 (Figure 5c) and compared them with ANNall. The national average MAD of Nr deposition for ANNemis17 (0.69 kg N ha^{-1} yr^{-1}) was closer to that of ANNall (0.91 kg N ha^{-1} yr^{-1}), while the MAD of ANNmeto17 (0.46) was half that of ANNall. Meanwhile, the spatial correlation (R) of MADs between ANNall and ANNemis17 reached 0.89 (Figure 5b), while it was less at 0.70 between ANNall and ANNmeto17 (Figure 5c), indicating that the IAVs of Nr deposition was mainly dominated by the changes of meteorology.

We further calculated the APDM of Nr deposition for ANNall, ANNemis17, and ANNmeto17 to evaluate the roles of anthropogenic emissions and meteorological conditions on IAVs in key regions. Figure 6 shows the seasonal averaged APDMs of dry deposition for NC, SC and SCB in the three scenarios. The driving factors of seasonal IAVs in dry deposition varied by region and species. Similar APDMs were found for DDEP_OXN in NC between ANNemis17 and ANNmeto17 for spring, summer and autumn, while the values for ANNmeto17 were slightly larger. The results indicated that the IAVs of DDEP_OXN were affected by both the changing meteorological conditions and emissions. In winter, the APDM of ANNemis17 was nearly twice of ANNmeto17 and close to that of ANNvall, indicating a more important role of meteorological variation on the IAVs of DDEP_OXN. For SC and SCB, the differences in APDMs of DDEP_OXN between ANNmeto17 and ANNemis17 were limited (within ±2%) in spring, autumn and winter, indicating similar effects of the changing meteorological conditions and emissions on IAVs of DDEP_OXN. In summer, the APDMs of ANNemis17 was much closer to that of ANNvall compared with ANNmeto17, indicating that the IAVs of DDEP_OXN was mainly driven by meteorological conditions.

For DDEP_RDN, the IAVs in winter in the NC region was mainly driven by the changing meteorological conditions (same as DDEP_OXN). In other seasons, the IAVs of DDEP_RDN were influenced by both the changing meteorological conditions and emissions. In contrast to DDEP_OXN, the changing emissions played a more important role indicated by the larger APDMs of ANNmeto17 than those of ANNemis17. Close APDMs between ANNemis17 and ANNmeto17 were found for all seasons in SC, indicating the similar contributions of both factors to the IAVs. In SCB, the IAVs in summer and winter were identified to be dominated by the changing meteorological conditions.

For wet deposition, as seen in Figure 7, similar APDMs was calculated for both OXN and RDN deposition in ANNall simulation, with the values ranging 13.22%–35.28%. The largest APDMs were generally found in autumn and winter, reflecting the stronger IAVs of precipitation in the seasons. With the changing meteorological conditions alone in ANNemis17 simulation, the APDMs ranged 12.89%–32.56%, very close to those in ANNall. In contrast, the APDMs calculated by the ANNmeto17 simulation were generally smaller than 10%, especially for

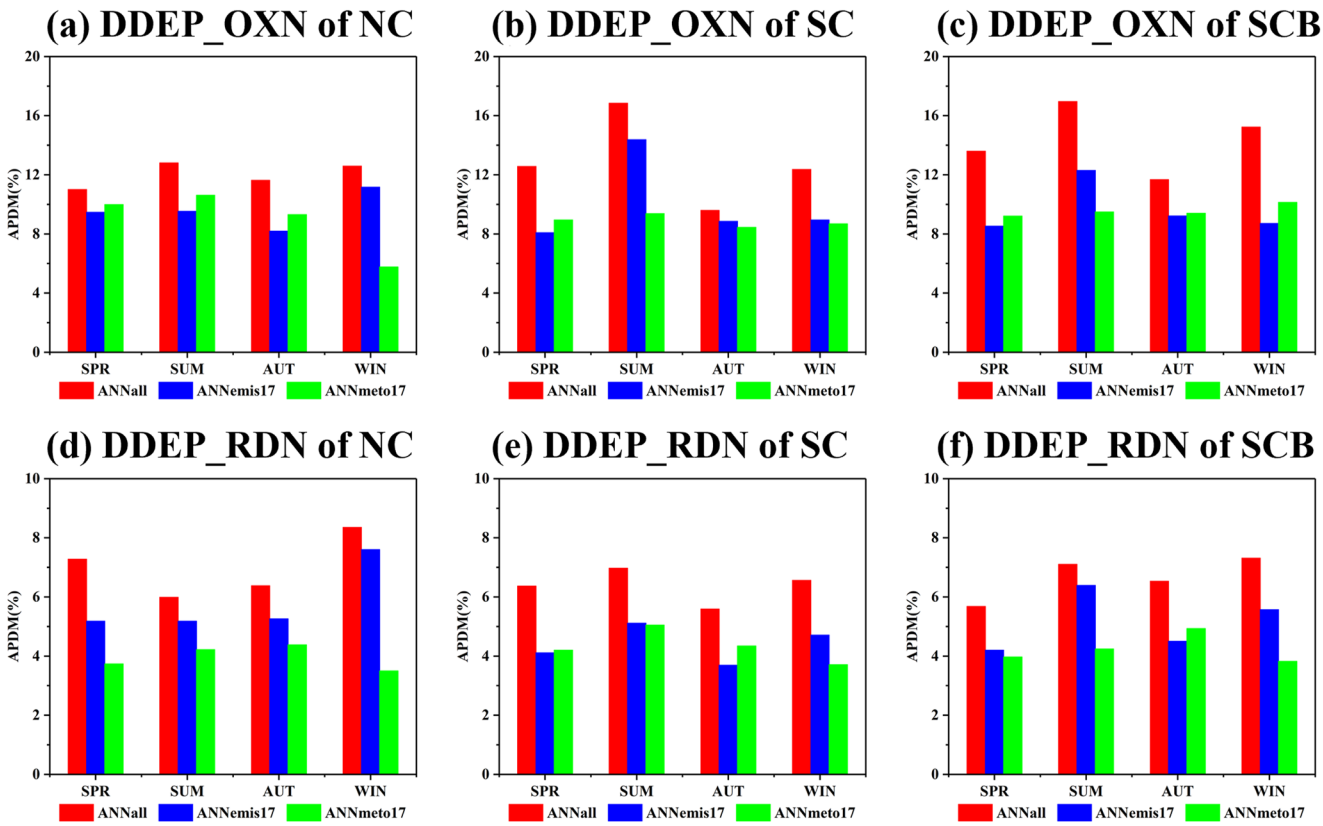

Figure 6. The seasonal domain-averaged absolute percent departure from the means (%) of DDEP_OXN (a–c) and DDEP_RDN (d–f) simulated in ANNall, ANNemis17 and ANNmeto17 over NC, SC and Sichuan Basin during 2008–2017.

WDEP_RDN. The comparison indicated the significant contributions of the changing meteorological conditions to the IAVs of wet deposition.

Figure 8 summarizes the relative contributions of changing emissions and meteorology to the trends and IAVs of Nr deposition from 2008 to 2017, estimated with Equations 9–12. The approach quantified the extent to which the changing emissions and meteorological conditions could explain the trend and IAVs of Nr deposition. As shown in Figure 8a, the changing emissions alone were estimated to explain 61 (NC)–83% (SCB) of the 10-year trends for the concerned regions, and thus to dominate the long-term trend in Nr deposition. The relative contribution was estimated at 75% at the national scale. The dominant factors influencing the 10-year trend of each Nr species (HNO_3, NH_3, particulate NO_3^- and particulate NH_4^+) are consistent with the findings for total Nr deposition, that is, emissions changes dominated the trend (Figures S9a–S9d in Supporting Information S1). The linear fitting results of annual Nr deposition for the concerned three regions in China are shown in Figure S10 in Supporting Information S1. At the national scale, the ICRs of the annual Nr deposition for ANNemis17 and ANNmeto17 scenarios were calculated at −0.019 and −0.068 kg N ha^{-1} yr^{-1}, respectively, indicating that meteorology and emissions jointly resulted in the decline of Nr deposition from 2008 to 2017 (the ICR for ANNall was −0.095 kg N ha^{-1} yr^{-1}). Similarly, emissions and meteorology were both estimated to contribute to Nr decline in NC, with the ICRs for ANNmeto17 and ANNemis17 at −0.26 and −0.18 kg N ha^{-1} yr^{-1}, respectively. For SC and SCB, in contrast, the ICRs in ANNemis17 were positive, suggesting that meteorological changes would enhance Nr deposition and thereby weaken the benefit of emission controls for the two regions during the research period. Furthermore, similar regional patterns were found for the trends in annual total precipitation (i.e., decline in NC and growth in SC and SCB, Figure S11 in Supporting Information S1) with those in Nr deposition from ANNemis17 simulation, indicating that precipitation could be an important meteorological factor influencing the trend of Nr deposition during 2008–2017.

Different from trend that dominated by emission change, the changing meteorological conditions played a significant role on the IAVs of Nr deposition, with the relative contributions estimated at approximately 60% for all the

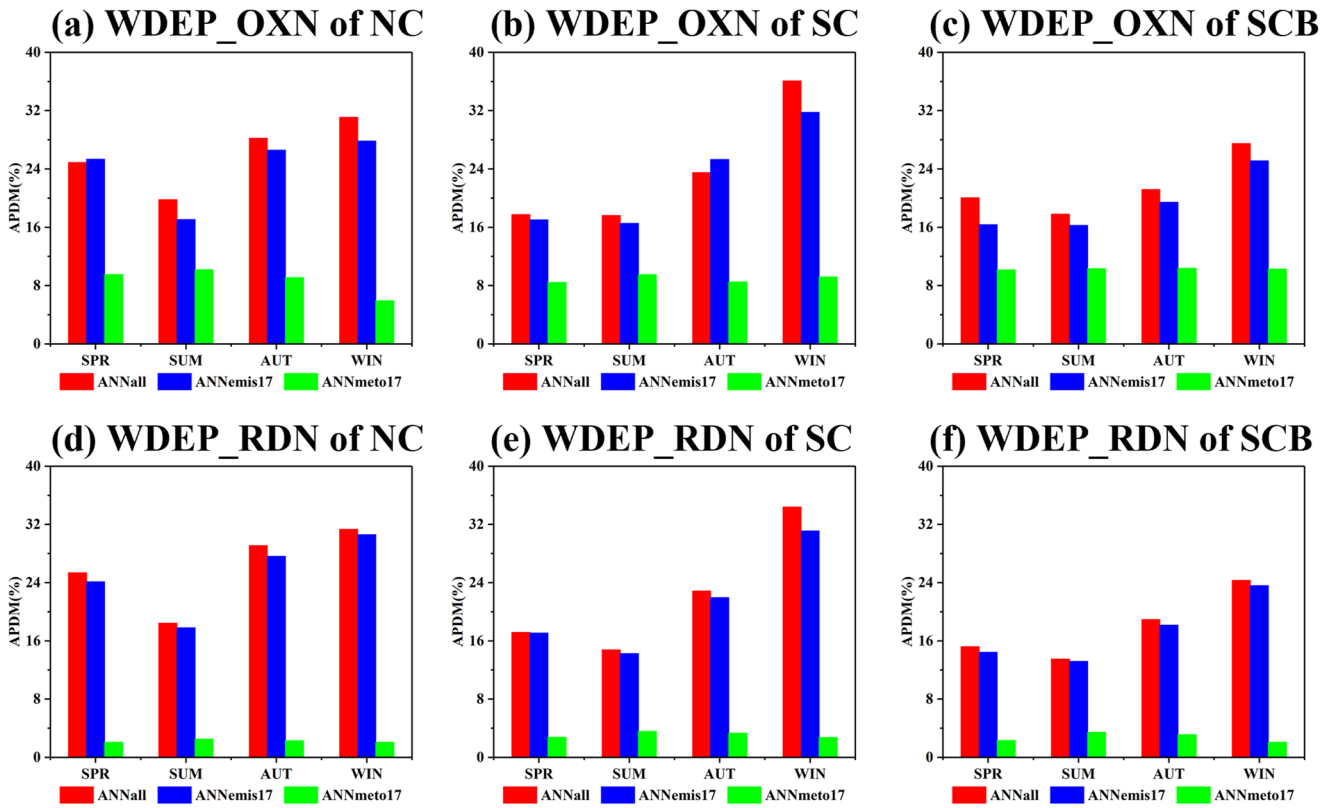

Figure 7. The seasonal domain-averaged APDMs (%) of WDEP_OXN (a–c) and WDEP_RDN (d–f) simulated in ANNall, ANNemis17, and ANNmeto17 over NC, SC, and Sichuan Basin during 2008–2017.

concerned regions (Figure 8b). More intense meteorological effects occurred for particulate NO_3^- deposition, with the relative contribution of meteorology factors for IAVs was always higher than that of other species deposition (66%–72% for particle NO_3^- deposition and 54%–64% for deposition of HNO_3, NH_3, and particulate NH_4^+) at national and sub-regional level (Figures S9d and S9e in Supporting Information S1). Among all the meteorological factors, the MAD of precipitation was found to be mostly correlated with that of annual Nr deposition, with a correlation coefficient of +0.47 for 2008–2017 (Figure S8 in Supporting Information S1). The result confirmed that the variation in precipitation was a major factor of the IAVs of Nr deposition.

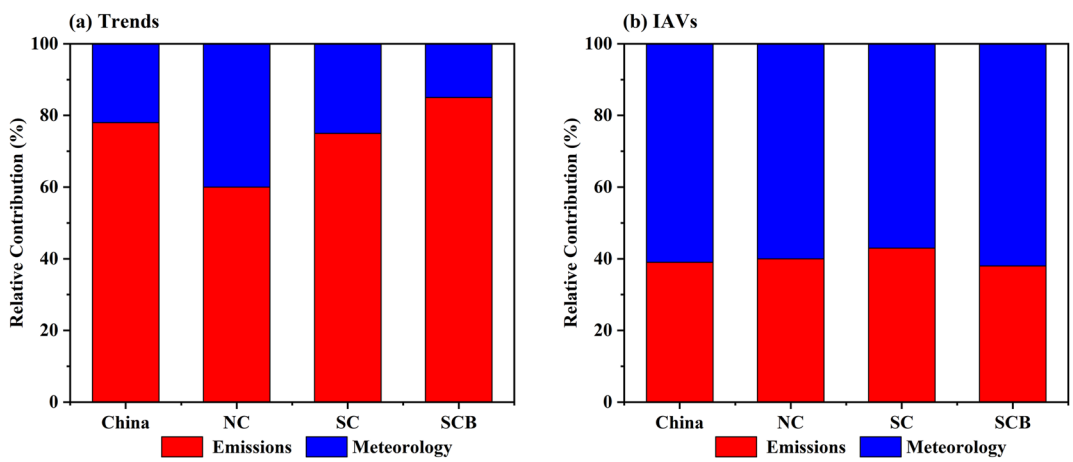

Figure 8. Relative contributions of changing emissions and meteorology to the trend (a) and interannual variations (b) of Nr deposition from 2008 to 2017.

Uncertainty existed when evaluating the relative contributions of meteorology changes and emission changes to the trend and IAVs of Nr deposition. On the one hand, the comparison between the simulations with fixed meteorology and emission scenario could not fully separate the interaction between the two factors, for example, NH_3 volatilization is strongly dependent on the ambient temperature, and the electricity or heating demand and thereby pollutant emissions vary associated with the temperature to support building cooling or warming. As an example, Abel et al. (2017) found a roughly 3% increase in electricity SO_2, NO_X and CO_2 emissions per °C increase in summer in the Eastern United States. For the total emissions form all sectors, this influence was modest. On the other hand, the response of Nr deposition is nonlinear to the changing meteorology and emissions, introducing extra bias in the analysis. Following Zhang et al. (2017) and Cheng et al. (2019), we quantified the impact of such nonlinear effect on the results (see Text Section 2 in the Supplement for detailed method). The bias was calculated at -2.0 kg N ha^{-1} yr^{-1}, accounting for -5.9% of simulated Nr deposition change during 2008–2017. Therefore, the uncertainty from nonlinear effect in the simulation was relatively small and would not affect the main findings of this study.

4. Conclusions

We conducted multi-year simulation with WRF-EMEP and explored the 10-year trend and IAVs of China's atmospheric Nr deposition for different deposition forms and species from 2008 to 2017. The annual mean Nr deposition for the 10 years was simulated at 15.7 ± 0.9 kg N ha^{-1} yr^{-1} all over the country. The ratio of RDN to OXN started to rise by 8% yr^{-1} after 2011, driven mainly by the continuous implementation of NO_X emission control policies, and China has been stepping into the RDN dominating condition in terms of Nr deposition.

With a least square piecewise linear fit, we found an increasing trend during 2008–2012 followed by a decline during 2013–2017 for all deposition forms and species, with the interannual changes in Nr deposition estimated at $+0.51$ and -0.39 Tg N yr^{-1} for the two periods, respectively. The trend in Nr deposition over the 10-year period resulted mainly from the changes in OXN, implying the benefit of the nationwide anthropogenic NO_X emission control on limiting the atmospheric nitrogen pollution and thereby relevant ecological impacts. For the spatial evolution of Nr deposition, SDE analysis indicated a significant shift to the southwest with the mean center point moving from (112.33°N, 33.06°E) to (111.88°N, 32.59°E) during 2013–2017, driven by the unequal variation of deposition in different regions. The IAVs of Nr deposition were quantified based on MAD and APDM, The MADs of Nr deposition during 2008–2017 ranged 0.01–9.2 kg N ha^{-1} yr^{-1} across the country, and clearly larger values existed in EC. The MADs of wet deposition were much higher than those of dry deposition, indicating the critical role of the former on IAVs of Nr deposition.

Compared to ANNmeto17 in which meteorology field was fixed for multi-year simulation, the magnitude and spatial distribution of MADs of Nr deposition for ANNemis17 in which emission input was fixed were more consistent with those of base simulation (ANNall), indicating the greater impact of changing meteorological conditions on IAVs of Nr deposition. However, emission changes were identified to be the major driver of the trend of Nr deposition during 2008–2017, with the normalized relative contribution ranging 61%–83% for the concerned regions across the country. This work reveals the effectiveness of China's emission control on Nr deposition for recent decade, and provides scientific basis for further understanding interannual trends in the ecological impact of nitrogen deposition.

Conflict of Interest

The authors declare no conflicts of interest relevant to this study.

Data Availability Statement

The NCEP 1° × 1° FNL are acquired from the website of (https://rda.ucar.edu/datasets/ds083.2/). (NCEP et al., 2000) [Dataset]. The MEIC and MIX emission inventory are available at http://meicmodel.org.cn/?page_id=560 and http://meicmodel.org.cn/?page_id=89, respectively (Li et al., 2017a; Li et al., 2017b; Zheng et al., 2018). [Dataset]. The ground meteorological observations could be obtained from the website: http://data.cma.cn/data/detail/dataCode/A.0012.0001.html [Dataset]. The observations of annual Nr deposition fluxes are taken from the NNDMN deposition data set from the website of https://doi.org/10.6084/m9.figshare.7451357 (Xu et al., 2019) [Dataset].

Acknowledgments
This study was jointly funded by the National Natural Science Foundation of China (42177080 and 41922052). We are grateful to the High Performance Computing Center (HPCC) of Nanjing University for doing the numerical calculations in this paper on its blade cluster system. We show our deepest respect and appreciation to the three anonymous reviewers for their insightful and constructive suggestions to help us largely improve the manuscript.

References

Abel, D., Holloway, T., Kladar, R. M., Meier, P., Ahl, D., Harkey, M., & Patz, J. (2017). Response of power plant emissions to ambient temperature in the eastern United States. *Environmental Science & Technology*, *51*(10), 5838–5846. https://doi.org/10.1021/acs.est.6b06201

Aber, J., McDowell, W., Nadelhoffer, K., Magill, A., Berntson, G., Kamakea, M., et al. (1998). Nitrogen saturation in temperate forest ecosystems. *BioScience*, *48*(11), 921–934. https://doi.org/10.2307/1313296

Bobbink, R., Hicks, K., Galloway, J., Spranger, T., Alkemade, R., Ashmore, M., et al. (2010). Global assessment of nitrogen deposition effects on terrestrial plant diversity: A synthesis. *Ecological Applications*, *20*(1), 30–59. https://doi.org/10.1890/08-1140.1

Carvalho, D., Rocha, A., Gómez-Gesteira, M., & Santos, C. (2012). A sensitivity study of the WRF model in wind simulation for an area of high wind energy. *Environmental Modelling & Software*, *33*, 23–34. https://doi.org/10.1016/j.envsoft.2012.01.019

Chang, M., Cao, J., Ma, M., Liu, Y., Liu, Y., Chen, W., et al. (2020). Dry deposition of reactive nitrogen to different ecosystems across eastern China: A comparison of three community models. *Science of The Total Environment*, *720*, 137548. https://doi.org/10.1016/j.scitotenv.2020.137548

Chen, H., Li, D., Gurmesa, G. A., Yu, G., Li, L., Zhang, W., et al. (2015). Effects of nitrogen deposition on carbon cycle in terrestrial ecosystems of China: A meta-analysis. *Environmental Pollution*, *206*, 352–360. https://doi.org/10.1016/j.envpol.2015.07.033

Chen, L., Xu, L., Cai, Y., & Yang, Z. (2021). Spatiotemporal patterns of industrial carbon emissions at the city level. *Resources, Conservation and Recycling*, *169*, 105499. https://doi.org/10.1016/j.resconrec.2021.105499

Chen, L., Xu, L., & Yang, Z. (2019). Inequality of industrial carbon emissions of the urban agglomeration and its peripheral cities: A case in the Pearl River Delta, China. *Renewable and Sustainable Energy Reviews*, *109*, 438–447. https://doi.org/10.1016/j.rser.2019.04.010

Cheng, J., Su, J., Cui, T., Li, X., Dong, X., Sun, F., et al. (2019). Dominant role of emission reduction in PM 2.5 air quality improvement in Beijing during 2013–2017: A model-based decomposition analysis. *Atmospheric Chemistry and Physics*, *19*(9), 6125–6146. https://doi.org/10.5194/acp-19-6125-2019

Civerolo, K. L., Hogrefe, C., Lynn, B., Rosenzweig, C., Goldberg, R., Rosenthal, J., et al. (2008). Simulated effects of climate change on summertime nitrogen deposition in the eastern US. *Atmospheric Environment*, *42*(9), 2074–2082. https://doi.org/10.1016/j.atmosenv.2007.11.049

CMA Meteorological Data Centre. (2022). Hourly meteorological data [Dataset]. CMA. Retrieved from http://data.cma.cn/data/detail/dataCode/A.0012.0001.html

Dang, R., Liao, H., & Fu, Y. (2021). Quantifying the anthropogenic and meteorological influences on summertime surface ozone in China over 2012–2017. *Science of The Total Environment*, *754*, 142394. https://doi.org/10.1016/j.scitotenv.2020.142394

Flechard, C. R., Nemitz, E., Smith, R. I., Fowler, D., Vermeulen, A. T., Bleeker, A., et al. (2011). Dry deposition of reactive nitrogen to European ecosystems: A comparison of inferential models across the NitroEurope network. *Atmospheric Chemistry and Physics*, *11*(6), 2703–2728. https://doi.org/10.5194/acp-11-2703-2011

Fowler, D., Coyle, M., Skiba, U., Sutton, M. A., Cape, J. N., Reis, S., et al. (2013). The global nitrogen cycle in the twenty-first century. *Philosophical Transactions of the Royal Society B: Biological Sciences*, *368*(1621), 20130164. https://doi.org/10.1098/rstb.2013.0164

Fu, Y., Liao, H., Tian, X., Gao, H., Cai, Z., & Han, R. (2019). Sensitivity of the simulated CO_2 concentration to inter-annual variations of its sources and sinks over East Asia. *Advances in Climate Change Research*, *10*(4), 250–263. https://doi.org/10.1016/j.accre.2020.03.001

Ge, B., Itahashi, S., Sato, K., Xu, D., Wang, J., Fan, F., et al. (2020). Model Inter-Comparison Study for Asia (MICS-Asia) phase III: Multimodel comparison of reactive nitrogen deposition over China. *Atmospheric Chemistry and Physics*, *20*(17), 10587–10610. https://doi.org/10.5194/acp-20-10587-2020

Geng, G., Xiao, Q., Liu, S., Liu, X., Cheng, J., Zheng, Y., et al. (2021). Tracking air pollution in China: Near real-time PM 2.5 retrievals from multisource data fusion. *Environmental Science & Technology*, *55*(17), 12106–12115. https://doi.org/10.1021/acs.est.1c01863

Geng, G., Xiao, Q., Zheng, Y., Tong, D., Zhang, Y., Zhang, X., et al. (2019). Impact of China's Air Pollution Prevention and Control Action Plan on $PM_{2.5}$ chemical composition over eastern China. *Science China Earth Sciences*, *62*(12), 1872–1884. https://doi.org/10.1007/s11430-018-9353-x

Gong, J. (2002). Clarifying the standard deviational ellipse. *Geographical Analysis*, *34*(2), 155–167. https://doi.org/10.1111/j.1538-4632.2002.tb01082.x

Greaver, T. L., Sullivan, T. J., Herrick, J. D., Barber, M. C., Baron, J. S., Cosby, B. J., et al. (2012). Ecological effects of nitrogen and sulfur air pollution in the US: What do we know? *Frontiers in Ecology and the Environment*, *10*(7), 365–372. https://doi.org/10.1890/110049

Gu, B., Ge, Y., Ren, Y., Xu, B., Luo, W., Jiang, H., et al. (2012). Atmospheric reactive nitrogen in China: Sources, recent trends, and damage costs. *Environmental Science & Technology*, *46*(17), 9420–9427. https://doi.org/10.1021/es301446g

He, K., Zhang, Q., & Wang, S. (2018). *Technical manual for the preparation of urban air pollution Source emission inventory*. China Statistics Press. (in Chinese).

Hertel, O., Skjøth, C. A., Løfstrøm, P., Geels, C., Frohn, L. M., Ellermann, T., & Madsen, P. V. (2006). Modelling nitrogen deposition on a local scale—A review of the current state of the art. *Environmental Chemistry*, *3*(5), 317. https://doi.org/10.1071/EN06038

Huang, Z., Wang, S., Zheng, J., Yuan, Z., Ye, S., & Kang, D. (2015). Modeling inorganic nitrogen deposition in Guangdong province, China. *Atmospheric Environment*, *109*, 147–160. https://doi.org/10.1016/j.atmosenv.2015.03.014

Itahashi, S., Ge, B., Sato, K., Fu, J. S., Wang, X., Yamaji, K., et al. (2020). MICS-Asia III: Overview of model intercomparison and evaluation of acid deposition over Asia. *Atmospheric Chemistry and Physics*, *20*(5), 2667–2693. https://doi.org/10.5194/acp-20-2667-2020

Kanakidou, M., Myriokefalitakis, S., Daskalakis, N., Fanourgakis, G., Nenes, A., Baker, A. R., et al. (2016). Past, present, and future atmospheric nitrogen deposition. *Journal of the Atmospheric Sciences*, *73*(5), 2039–2047. https://doi.org/10.1175/JAS-D-15-0278.1

Kang, Y., Liu, M., Song, Y., Huang, X., Yao, H., Cai, X., et al. (2016). High-resolution ammonia emissions inventories in China from 1980 to 2012. *Atmospheric Chemistry and Physics*, *16*(4), 2043–2058. https://doi.org/10.5194/acp-16-2043-2016

Li, B., Chen, L., Shen, W., Jin, J., Wang, T., Wang, P., et al. (2021). Improved gridded ammonia emission inventory in China. *Atmospheric Chemistry and Physics*, *21*(20), 15883–15900. https://doi.org/10.5194/acp-21-15883-2021

Li, M., Liu, H., Geng, G., Hong, C., Liu, F., Song, Y., et al. (2017). Anthropogenic emission inventories in China: A review. *National Science Review*, *4*(6), 834–866. https://doi.org/10.1093/nsr/nwx150

Li, M., Zhang, Q., Kurokawa, J., Woo, J. H., He, K., Lu, Z., et al. (2017). MIX: A mosaic Asian anthropogenic emission inventory under the international collaboration framework of the MICS-Asia and HTAP. *Atmospheric Chemistry and Physics*, *17*(2), 935–963. https://doi.org/10.5194/acp-17-935-2017

Li, Y., Schichtel, B. A., Walker, J. T., Schwede, D. B., Chen, X., Lehmann, C. M., et al. (2016). Increasing importance of deposition of reduced nitrogen in the United States. *Proceedings of the National Academy of Sciences*, *113*(21), 5874–5879. https://doi.org/10.1073/pnas.1525736113

Liu, L., & Greaver, T. L. (2009). A review of nitrogen enrichment effects on three biogenic GHGs: The CO_2 sink may be largely offset by stimulated N_2O and CH_4 emission. *Ecology Letters*, *12*(10), 1103–1117. https://doi.org/10.1111/j.1461-0248.2009.01351.x

Liu, M., Huang, X., Song, Y., Tang, J., Cao, J., Zhang, X., et al. (2019). Ammonia emission control in China would mitigate haze pollution and nitrogen deposition, but worsen acid rain. *Proceedings of the National Academy of Sciences*, *116*(16), 7760–7765. https://doi.org/10.1073/pnas.1814880116

Liu, X., & Du, E. (2020). An overview of atmospheric reactive nitrogen in China from a global perspective. In *Atmospheric reactive nitrogen in China* (pp. 1–10). Springer Singapore. https://doi.org/10.1007/978-981-13-8514-8_1

Liu, X., Duan, L., Mo, J., Du, E., Shen, J., Lu, X., et al. (2011). Nitrogen deposition and its ecological impact in China: An overview. *Environmental Pollution*, *159*(10), 2251–2264. https://doi.org/10.1016/j.envpol.2010.08.002

Liu, X., Xu, W., Duan, L., Du, E., Pan, Y., Lu, X., et al. (2017). Erratum to: Atmospheric nitrogen emission, deposition, and air quality impacts in China: An overview. *Current Pollution Reports*, *3*(2), 78. https://doi.org/10.1007/s40726-017-0056-6

Liu, X., Xu, W., Liu, L., Du, E., Shen, J., Luo, X., et al. (2020). Monitoring atmospheric nitrogen deposition in China. In *Atmospheric reactive nitrogen in China* (pp. 41–65). Springer Singapore. https://doi.org/10.1007/978-981-13-8514-8_3

Liu, X., Zhang, Y., Han, W., Tang, A., Shen, J., Cui, Z., et al. (2013). Enhanced nitrogen deposition over China. *Nature*, *494*(7438), 459–462. https://doi.org/10.1038/nature11917

Liu, Y., & Wang, T. (2020). Worsening urban ozone pollution in China from 2013 to 2017—Part 1: The complex and varying roles of meteorology. *Atmospheric Chemistry and Physics*, *20*(11), 6305–6321. https://doi.org/10.5194/acp-20-6305-2020

Ma, M., Chen, W., Jia, S., Chang, M., Zhong, B., & Wang, X. (2020). A new method for quantification of regional nitrogen emission—Deposition transmission in China. *Atmospheric Environment*, *227*, 117401. https://doi.org/10.1016/j.atmosenv.2020.117401

Mao, Y., Liao, H., Han, Y., & Cao, J. (2016). Impacts of meteorological parameters and emissions on decadal and interannual variations of black carbon in China for 1980-2010. *Journal of Geophysical Research: Atmospheres*, *121*(4), 1822–1843. https://doi.org/10.1002/2015JD024019

Matson, P., Lohse, K. A., & Hall, S. J. (2002). The globalization of nitrogen deposition: Consequences for terrestrial ecosystems. *Ambio*, *31*(2), 113–119. https://doi.org/10.1579/0044-7447-31.2.113

Melillo, J. M. (2021). Disruption of the global nitrogen cycle: A grand challenge for the twenty-first century. *Ambio*, *50*(4), 759–763. https://doi.org/10.1007/s13280-020-01429-2

Mu, Q., & Liao, H. (2014). Simulation of the interannual variations of aerosols in China: Role of variations in meteorological parameters. *Atmospheric Chemistry and Physics*, *14*(18), 9597–9612. https://doi.org/10.5194/acp-14-9597-2014

National Centers for Environmental Prediction/National Weather Service/NOAA/U.S. Department of Commerce. (2000). NCEP FNL operational model global tropospheric analyses, continuing from July 1999 [Dataset]. Research Data Archive at the National Center for Atmospheric Research, Computational and Information Systems Laboratory (updated daily). https://doi.org/10.5065/D6M043C6

Pan, Y., Tian, S., Zhao, Y., Zhang, L., Zhu, X., Gao, J., et al. (2018). Identifying ammonia hotspots in China using a national observation network. *Environmental Science & Technology*, *52*(7), 3926–3934. https://doi.org/10.1021/acs.est.7b05235

Peng, J., Chen, S., Lü, H., Liu, Y., & Wu, J. (2016). Spatiotemporal patterns of remotely sensed PM2.5 concentration in China from 1999 to 2011. *Remote Sensing of Environment*, *174*, 109–121. https://doi.org/10.1016/j.rse.2015.12.008

Shen, X., Yao, Z., Zhang, Q., Wagner, D. V., Huo, H., Zhang, Y., et al. (2015). Development of database of real-world diesel vehicle emission factors for China. *Journal of Environmental Sciences*, *31*, 209–220. https://doi.org/10.1016/j.jes.2014.10.021

Shen, Y., Jiang, F., Feng, S., Zheng, Y., Cai, Z., & Lyu, X. (2021). Impact of weather and emission changes on NO_2 concentrations in China during 2014–2019. *Environmental Pollution*, *269*(15), 116163. https://doi.org/10.1016/j.envpol.2020.116163

Shi, Y., Matsunaga, T., Yamaguchi, Y., Li, Z., Gu, X., & Chen, X. (2018). Long-term trends and spatial patterns of satellite-retrieved PM2.5 concentrations in South and Southeast Asia from 1999 to 2014. *Science of The Total Environment*, *615*, 177–186. https://doi.org/10.1016/j.scitotenv.2017.09.241

Shi, Y., Matsunaga, T., Yamaguchi, Y., Zhao, A., Li, Z., & Gu, X. (2018). Long-term trends and spatial patterns of PM2.5-induced premature mortality in South and Southeast Asia from 1999 to 2014. *Science of The Total Environment*, *631–632*, 1504–1514. https://doi.org/10.1016/j.scitotenv.2018.03.146

Simpson, D., Benedictow, A., Berge, H., Bergström, R., Emberson, L. D., Fagerli, H., et al. (2012). The EMEP MSC-W chemical transport model—Technical description. *Atmospheric Chemistry and Physics*, *12*(16), 7825–7865. https://doi.org/10.5194/acp-12-7825-2012

Tan, J., Fu, J. S., & Seinfeld, J. H. (2020). Ammonia emission abatement does not fully control reduced forms of nitrogen deposition. *Proceedings of the National Academy of Sciences*, *117*(18), 9771–9775. https://doi.org/10.1073/pnas.1920068117

van der Swaluw, E., de Vries, W., Sauter, F., Wichink Kruit, R., Vieno, M., Fagerli, H., & van Pul, A. (2021). Trend analysis of reduced nitrogen components over The Netherlands with the EMEP4NL and OPS model. *Atmospheric Environment*, *248*, 118183. https://doi.org/10.1016/j.atmosenv.2021.118183

Vet, R., Artz, R. S., Carou, S., Shaw, M., Ro, C.-U., Aas, W., et al. (2014). A global assessment of precipitation chemistry and deposition of sulfur, nitrogen, sea salt, base cations, organic acids, acidity and pH, and phosphorus. *Atmospheric Environment*, *93*, 3–100. https://doi.org/10.1016/j.atmosenv.2013.10.060

Wachowicz, M., & Liu, T. (2016). Finding spatial outliers in collective mobility patterns coupled with social ties. *International Journal of Geographical Information Science*, *30*(9), 1806–1831. https://doi.org/10.1080/13658816.2016.1144887

Wang, B., Shi, W., & Miao, Z. (2015). Confidence analysis of standard deviational ellipse and its extension into higher dimensional Euclidean space. *PLoS One*, *10*(3), e0118537. https://doi.org/10.1371/journal.pone.0118537

Wen, Z., Xu, W., Li, Q., Han, M., Tang, A., Zhang, Y., et al. (2020). Changes of nitrogen deposition in China from 1980 to 2018. *Environment International*, *144*, 106022. https://doi.org/10.1016/j.envint.2020.106022

Werner, M., Kryza, M., & Wind, P. (2018). High resolution application of the EMEP MSC-W model over Eastern Europe—Analysis of the EMEP4PL results. *Atmospheric Research*, *212*, 6–22. https://doi.org/10.1016/j.atmosres.2018.04.025

Wu, N., Geng, G., Yan, L., Bi, J., Li, Y., Tong, D., et al. (2019). Improved spatial representation of a highly resolved emission inventory in China: Evidence from TROPOMI measurements. *Environmental Research Letters*, *16*(8), 084056. https://doi.org/10.1088/1748-9326/ac175f

Xiao, Q., Zheng, Y., Geng, G., Chen, C., Huang, X., Che, H., et al. (2021). Separating emission and meteorological contributions to long-term $PM_{2.5}$ trends over eastern China during 2000-2018. *Atmospheric Chemistry and Physics*, *21*(12), 9475–9496. https://doi.org/10.5194/acp-21-9475-2021

Xu, W., Liu, L., Cheng, M., Zhao, Y., Zhang, L., Pan, Y., et al. (2018). Spatial–temporal patterns of inorganic nitrogen air concentrations and deposition in eastern China. *Atmospheric Chemistry and Physics*, *18*(5), 10931–10954. https://doi.org/10.5194/acp-18-10931-2018

Xu, W., Zhang, L., & Liu, X. (2019). A database of atmospheric nitrogen concentration and deposition from the nationwide monitoring network in China. *Scientific Data*, *6*(1), 51. https://doi.org/10.1038/s41597-019-0061-2

Yang, D., Luan, W., Qiao, L., & Pratama, M. (2020). Modeling and spatio-temporal analysis of city-level carbon emissions based on nighttime light satellite imagery. *Applied Energy*, *268*, 114696. https://doi.org/10.1016/j.apenergy.2020.114696

Yang, Y., Liao, H., & Lou, S. (2015). Decadal trend and interannual variation of outflow of aerosols from East Asia: Roles of variations in meteorological parameters and emissions. *Atmospheric Environment*, *100*, 141–153. https://doi.org/10.1016/j.atmosenv.2014.11.004

Yu, G., Jia, Y., He, N., Zhu, J., Chen, Z., Wang, Q., et al. (2019). Stabilization of atmospheric nitrogen deposition in China over the past decade. *Nature Geoscience*, *12*(6), 424–429. https://doi.org/10.1038/s41561-019-0352-4

Yu, L., Yin, C., Lin, Y., & He, J. (2017). Study of dynamical downscaling on near surface wind speed over China. *Journal of Arid Meteorology*, *35*(1), 23–28. Retrieved from http://www.ghqx.org.cn/EN/10.11755/j.issn.1006-7639(2017)-01-0023

Yue, P., Cui, X., Gong, Y., Li, K., Goulding, K., & Liu, X. (2019). Fluxes of N_2O, CH_4 and soil respiration as affected by water and nitrogen addition in a temperate desert. *Geoderma*, *337*, 770–772. https://doi.org/10.1016/j.geoderma.2018.10.020

Zhang, L., Chen, Y., Zhao, Y., Henze, D. K., Zhu, L., Song, Y., et al. (2018). Agricultural ammonia emissions in China: Reconciling bottom-up and top-down estimates. *Atmospheric Chemistry and Physics*, *18*(1), 339–355. https://doi.org/10.5194/acp-18-339-2018

Zhang, Q., Jiang, X., Tong, D., Davis, S. J., Zhao, H., Geng, G., et al. (2017). Transboundary health impacts of transported global air pollution and international trade. *Nature*, *543*(7647), 705–709. https://doi.org/10.1038/nature21712

Zhao, B., Wang, S. X., Liu, H., Xu, J. Y., Fu, K., Klimont, Z., et al. (2013). NOx emissions in China: Historical trends and future perspectives. *Atmospheric Chemistry and Physics*, *13*(19), 9869–9897. https://doi.org/10.5194/acp-13-9869-2013

Zhao, Y., Xi, M., Zhang, Q., Dong, Z., Ma, M., Zhou, K., et al. (2022). Decline in bulk deposition of air pollutants in China lags behind reductions in emissions. *Nature Geoscience*, *15*(3), 190–195. https://doi.org/10.1038/s41561-022-00899-1

Zhao, Y., Zhang, L., Chen, Y., Liu, X., Xu, W., Pan, Y., & Duan, L. (2017). Atmospheric nitrogen deposition to China: A model analysis on nitrogen budget and critical load exceedance. *Atmospheric Environment*, *153*, 32–40. https://doi.org/10.1016/j.atmosenv.2017.01.018

Zhao, Y., Zhang, L., Pan, Y., Wang, Y., Paulot, F., & Henze, D. K. (2015). Atmospheric nitrogen deposition to the northwestern Pacific: Seasonal variation and source attribution. *Atmospheric Chemistry and Physics*, *15*(18), 10905–10924. https://doi.org/10.5194/acp-15-10905-2015

Zheng, B., Tong, D., Li, M., Liu, F., Hong, C., Geng, G., et al. (2018). Trends in China's anthropogenic emissions since 2010 as the consequence of clean air actions. *Atmospheric Chemistry and Physics*, *18*(19), 14095–14111. https://doi.org/10.5194/acp-18-14095-2018

Zhu, J., Liao, H., Mao, Y., Yang, Y., & Jiang, H. (2017). Interannual variation, decadal trend, and future change in ozone outflow from East Asia. *Atmospheric Chemistry and Physics*, *17*(5), 3729–3747. https://doi.org/10.5194/acp-17-3729-2017

Zhu, K., Yu, B., Xue, M., Zhou, B., & Hu, X. (2021). Summer season precipitation biases in 4 km WRF forecasts over southern China: Diagnoses of the causes of biases. *Journal of Geophysical Research: Atmospheres*, *126*(23). https://doi.org/10.1029/2021JD035530

References From the Supporting Information

Chen, F., Miao, S., Tewari, M., Bao, J., & Kusaka, H. (2011). A numerical study of interactions between surface forcing and sea breeze circulations and their effects on stagnation in the greater Houston area. *Journal of Geophysical Research*, *116*, D12105. https://doi.org/10.1029/2010JD015533

Chou, M. D., & Suarez, M. J. (1994). An efficient thermal infrared radiation parameterization for use in general circulation models (NASA Tech: Memorandum, NASA/TM-1994-104606).

Goodarzi, L., Banihabib, M. E., & Roozbahani, A. (2019). A decision-making model for flood warning system based on ensemble forecasts. *Journal of Hydrology*, *573*, 207–219. https://doi.org/10.1016/j.jhydrol.2019.03.040

Han, X., Zhang, M., Skorokhod, A., & Kou, X. (2017). Modeling dry deposition of reactive nitrogen in China with RAMS-CMAQ. *Atmospheric Environment*, *166*, 47–61. https://doi.org/10.1016/j.atmosenv.2017.07.015

Hong, S., Noh, Y., & Dudhia, J. (2006). A new vertical diffusion package with an explicit treatment of entrainment processes. *Monthly Weather Review*, *134*(9), 2318–2341. https://doi.org/10.1175/MWR3199.1

Iacono, M. J., Delamere, J. S., Mlawer, E. J., Shephard, M. W., Clough, S. A., & Collins, W. D. (2008). Radiative forcing by long-lived greenhouse gases: Calculations with the AER radiative transfer models. *Journal of Geophysical Research*, *113*(D13), D13103. https://doi.org/10.1029/2008JD009944

Lin, Y., Farley, R. D., & Orville, H. D. (1983). Bulk parameterization of the snow field in a cloud model. *Journal of Applied Meteorology and Climatology*, *22*(6), 1065–1092. https://doi.org/10.1175/1520-0450(1983)022<1065:BPOTSF>2.0.CO;2

Niu, G., Yang, Z., Mitchell, K. E., Chen, F., Ek, M. B., Barlage, M., et al. (2011). The community Noah land surface model with multiparameterization options (Noah-MP): 1. Model description and evaluation with local-scale measurements. *Journal of Geophysical Research*, *116*(D12), D12109. https://doi.org/10.1029/2010JD015139

Xu, W., Luo, X., Pan, Y., Zhang, L., Tang, A., Shen, J., et al. (2015). Quantifying atmospheric nitrogen deposition through a nationwide monitoring network across China. *Atmospheric Chemistry and Physics*, *15*(21), 12345–12360. https://doi.org/10.1029/acp-15-12345-2015